

Fully anisotropic finite strain viscoelasticity based on a reverse multiplicative decomposition and logarithmic strains

Marcos Latorre, Francisco Javier Montáns*

*Escuela Técnica Superior de Ingeniería Aeronáutica y del Espacio
Universidad Politécnica de Madrid
Plaza Cardenal Cisneros, 3, 28040-Madrid, Spain*

Abstract

In this paper we present a novel formulation for phenomenological anisotropic finite visco-hyperelasticity. The formulation is based on a multiplicative decomposition of the equilibrated deformation gradient into nonequilibrated elastic and viscous contributions. The proposal in this paper is a decomposition reversed respect to that from Sidoroff allowing for anisotropic viscous contributions. Independent anisotropic stored energies are employed for equilibrated and non-equilibrated parts. The formulation uses logarithmic strain measures in order to be teamed with spline-based hyperelasticity. Some examples compare the results with formulations that use the Sidoroff decomposition and also show the enhanced capabilities of the present model.

Keywords: Viscoelasticity; Hyperelasticity; Logarithmic strains; Anisotropy; Polymers; Biological tissues.

*Corresponding author. Tel.:+34 637 908 304.

Email addresses: m.latorre.ferrus@upm.es (Marcos Latorre), fco.montans@upm.es (Francisco Javier Montáns)

1. Introduction

Rubberlike materials and biological tissues are capable of sustaining large strains and are frequently considered quasi-incompressible and hyperelastic in finite element analyses, see for example [1, 2, 3, 4, 5, 6, 7]. In the observed behavior of these materials, specially in biological tissues, there is frequently a relevant viscous component [3, 4]. Hence, visco-hyperelastic models are very important in both the engineering and biomechanics fields.

Among the many types of formulations proposed for isochoric viscoelasticity, two approaches stand out in finite element simulations. The first one was advocated by Simo [6, 8] and successfully used by other researchers, see [3, 9, 10, 11, 12], among others. This formulation is based on stress-like internal variables and allows for anisotropic stored energies. However, this formulation is not adequate for large deviations from thermodynamical equilibrium [13, 14] (i.e. *finite linear viscoelasticity*). Furthermore, the instantaneous and relaxed stored energies are usually proportional [6, 8].

The second approach has been proposed by Reese and Govindjee [13] and used also in References [15] and [16] among others. In this approach the Sidoroff multiplicative decomposition [17] is employed and the stored energy is separated into equilibrated and nonequilibrated parts following the framework introduced by Lubliner [18]. The main advantage of this formulation is that it is valid for deformations away from thermodynamical equilibrium and that distinct instantaneous and relaxed stored energies may be considered. As a drawback, the phenomenological formulation is only valid for isotropy, although anisotropic formulations are possible following these ideas and modelling the microstructure [19].

Recently we have developed a formulation following the ideas from Reese and

Govindjee which is valid for anisotropic hyperelasticity and for deformations arbitrarily away from thermodynamic equilibrium (i.e. *finite nonlinear viscoelasticity*) [20]. This formulation uses the Sidoroff multiplicative decomposition of the total (equilibrated) deformation gradient into non-equilibrated elastic and viscous parts. The equilibrated and non-equilibrated stored energies are formulated in terms of logarithmic strains. These strain measures are intuitive [21, 22, 23] and allow for simple formulations in large strain elasto-plasticity [26, 24, 25]. Furthermore, they are employed in spline-based hyperelasticity [27, 28, 29]. Spline-based hyperelasticity introduced by Sussman and Bathe permits the exact (in practice) replication of experimental data and also facilitates the interpretation of the material behavior [20] in visco-hyperelasticity. Furthermore, it may be formulated as to preserve both theoretical and numerical material symmetries consistency [30]. However, the inconvenience of the formulation of Reference [20] based on Sidoroff’s decomposition is that whereas the stored energies may be anisotropic, the viscous component should arguably be isotropic. This is due to the intermediate configuration imposed by the Sidoroff multiplicative decomposition. Hence, only one relaxation time can be considered as an independent parameter (i.e. obtained from an experiment). The relaxation times for the remaining components are given by the prescribed stored energies [20].

The purpose of this paper is to present a formulation for anisotropic visco-hyperelasticity in which both the stored energies and the viscous contribution are anisotropic. Therefore, in orthotropy up to six independent relaxation times may be independently prescribed, i.e. obtained from six different experiments as for the case of isochoric spline-based orthotropic equilibrated and nonequilibrated stored energies [29]. The procedure employs a reversed multiplicative decomposition from that used by Sidoroff. The intermediate configuration from this decomposition allows for

the formulation of the stored energies using the same structural tensors and, hence, facilitates the use of anisotropic viscosity tensors. The algorithm is introduced using a special co-rotational formulation in order to facilitate a parallelism with the formulation introduced in Reference [20]. As an inconvenience of the present formulation when compared to the one presented in [20], the resulting non-equilibrated consistent tangent moduli tensor is slightly non-symmetric for off-axis nonproportional loading. However, for the numerical nonproportional examples presented in this paper typically only one additional iteration is employed when using a symmetrized tensor. For the case of nonproportional off-axes loading, the observed behavior is also slightly different due to the also different multiplicative decomposition employed. Therefore, if the viscosity is considered isotropic, the formulation given in [20] may be preferred, but for more general anisotropic viscosities, the present formulation must be employed.

In this paper we focus mainly on the large strain formulation using the reversed decomposition. For a detailed small strains motivation and for some concepts used in the kinematics of the multiplicative decomposition, the reader can refer to Reference [20].

2. Sidoroff's and Reverse multiplicative decompositions

Unidimensional viscoelasticity is motivated by the standard solid rheological model [6], see Figure 1, where the small elongations of the springs and the viscous dashpot per unit device-length (i.e. infinitesimal strains) are related through

$$\varepsilon = \varepsilon_e + \varepsilon_v \tag{1}$$

Within the context of three-dimensional large deformations, a generalization of this additive decomposition in terms of some finite deformation measure is needed as point of departure in order to formulate strain-based constitutive viscoelastic models. One possibility was proposed by Sidoroff [17], who considered a multiplicative decomposition of the deformation gradient motivated on the similar Lee multiplicative decomposition in elastoplasticity [31, 32] —note that this tensor is usually written as \mathbf{F} , but we adopt the notation given in Ref. [1]

$$\mathbf{X} = \mathbf{X}_e \mathbf{X}_v \tag{2}$$

where \mathbf{X}_v includes the viscous contribution to the total deformation from the reference state to time t and \mathbf{X}_e accounts for the remaining elastic (nonequibrated) contribution, see Figure 1. Motivated on the standard solid of Figure 1, the intermediate state may be interpreted as the internal, non-equilibrated “stress-free” configuration obtained by the virtual elastic unloading of the *equivalent* Maxwell element from the current configuration by means of \mathbf{X}_e^{-1} [33]. The hypothetically relaxed total gradient is $\mathbf{X}^* = \mathbf{X}_e^{-1} \mathbf{X} = \mathbf{X}_v$. However, as a clear difference with finite elastoplasticity, note that this internal unloading is only fictitious even under homogeneous deformations (i.e. the intermediate configuration is not strictly speaking a “stress-free” configuration). The presence of an elastic deformation gradient makes the system to be internally unbalanced, so the system is continuously evolving in order to reach thermodynamic equilibrium in the sense that $\mathbf{X}_e \rightarrow \mathbf{I}$ and $\mathbf{X}_v \rightarrow \mathbf{X}$, for a given (fixed) total gradient \mathbf{X} . Hence, the intermediate configuration is truly relaxed only when internal static equilibrium is attained. In that case, note that the intermediate configuration has relaxed to (is coincident to) the actual configuration, i.e. $\mathbf{X} = \mathbf{I} \mathbf{X}_v$ at $t \rightarrow \infty$.

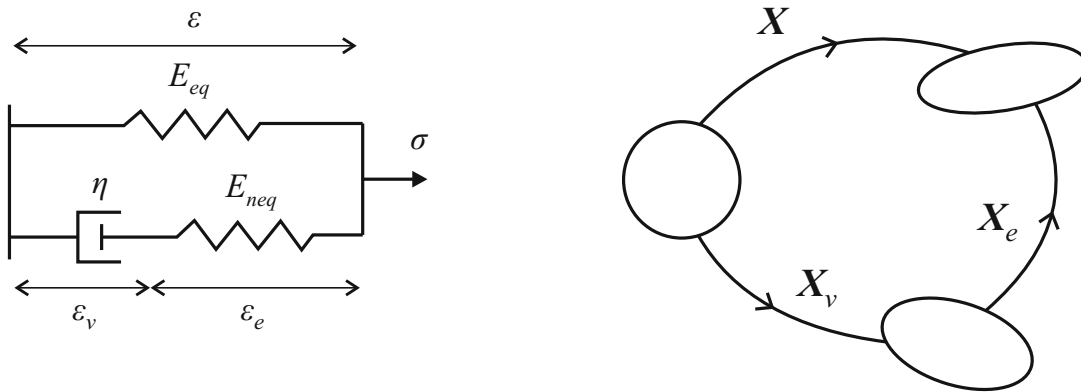


Figure 1: Sidoroff's multiplicative decomposition of the deformation gradient $\mathbf{X} = \mathbf{X}_e \mathbf{X}_v$. Left: Equivalent standard linear solid. Right: Sidoroff multiplicative decomposition

Consider now the standard solid of Figure 2. Of course, due to the additive decomposition used in infinitesimal viscoelasticity, the mechanical devices of Figures 1 and 2 may be considered equivalent from a *quantitative* standpoint. That is, the same model for the small strains unidimensional case [20] is obtained in both cases. However, they admit different physical interpretations even for the small strains case. Furthermore, they lead to different formulations in the large strains setting. The extension of the rheological model shown in Figure 2 to the finite deformation context is given by the *reversed* multiplicative decomposition of the deformation gradient

$$\mathbf{X} = \mathbf{X}_v \mathbf{X}_e \quad (3)$$

where \mathbf{X}_e includes the elastic contribution to the total deformation from the reference state to time t and \mathbf{X}_v accounts for the remaining viscous contribution. An apparent difference with the multiplicative decomposition of Figure 1 is that in this second case, the virtual elastic unloading of the *equivalent* Maxwell element is performed from the intermediate configuration to the reference configuration by means of \mathbf{X}_e^{-1} .

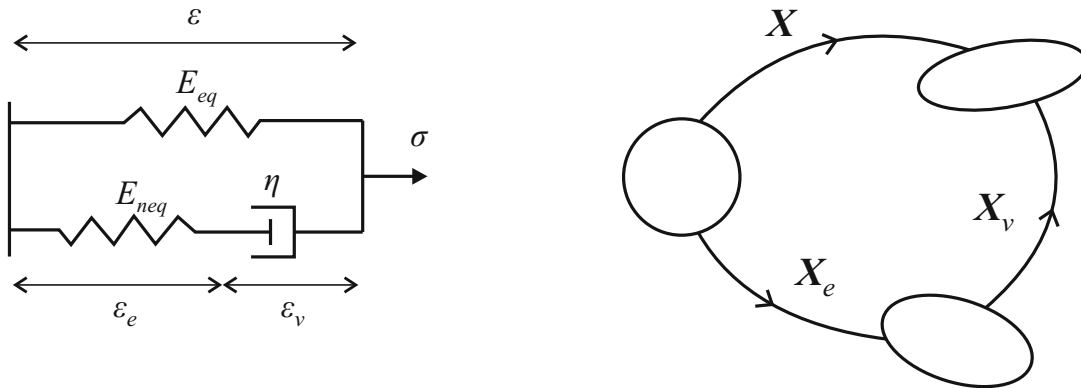


Figure 2: Reverse multiplicative decomposition of the deformation gradient $\mathbf{X} = \mathbf{X}_v \mathbf{X}_e$. Left: Equivalent standard linear solid. Right: Reverse multiplicative decomposition

The same hypothetically relaxed total gradient is obtained $\mathbf{X}^* = (\mathbf{X}_v \mathbf{X}_e^{-1} \mathbf{X}_v^{-1}) \mathbf{X} = \mathbf{X}_v$ in this case (we emphasize that these situations are only fictitious). However, for a fixed total gradient \mathbf{X} the intermediate configuration will have “relaxed” to (will be coincident to) the reference configuration, i.e. $\mathbf{X} = \mathbf{X}_v \mathbf{I}$ at $t \rightarrow \infty$, which become the main difference between both multiplicative decompositions.

Viscoelasticity formulations based on strain-like internal variables are built on the hypothesis of the existence of a strain energy density containing an equilibrated contribution and a non-equilibrated one [18, 13]. Given a multiplicative decomposition of the deformation gradient \mathbf{X} into an elastic part \mathbf{X}_e and a viscous one \mathbf{X}_v , the total stored energy function Ψ is therefore written as

$$\Psi = \Psi_{eq}(\mathbf{A}) + \Psi_{neq}(\mathbf{A}_e) \quad (4)$$

where \mathbf{A} and \mathbf{A}_e are the Green-Lagrange strain tensors obtained from the total deformation gradient \mathbf{X} and the internal elastic gradient \mathbf{X}_e , respectively. Of course, Ψ_{eq} and Ψ_{neq} may be expressed in terms of other Lagrangian strain measures. However,

we employ for now quadratic strain measures because they facilitate the analytical derivation of the material formulation, as we show in the following section.

There exists a crucial difference in the non-equilibrated part of the constitutive hypothesis given in Eq.(4) when one uses either the Sidoroff or the reverse multiplicative decomposition of the deformation gradient \mathbf{X} . On the one hand, if $\mathbf{X} = \mathbf{X}_e \mathbf{X}_v$, the non-equilibrated Green-Lagrange strains \mathbf{A}_e and the strain energy function Ψ_{neq} are both defined in the intermediate configuration. Hence, the second Piola-Kirchhoff stresses that directly derive from Ψ_{neq} (i.e. $\mathbf{S}_{neq}^{le} = d\Psi_{neq}/d\mathbf{A}_e$, using the notation introduced in Ref. [20]) also operates in that configuration. On the other hand, if $\mathbf{X} = \mathbf{X}_v \mathbf{X}_e$, both \mathbf{A}_e and Ψ_{neq} are defined in the reference configuration and \mathbf{S}_{neq}^{le} operates in the reference configuration as well. This consideration will show relevant when deriving the constitutive equation for the viscous flow in Section 5.1.

3. Finite strain viscoelasticity based on the reversed decomposition

In Ref. [20] we derived a computational model for finite fully non-linear anisotropic visco-hyperelasticity based on the Sidoroff's multiplicative decomposition of the deformation gradient given in Eq. (2). Departing from this kinematical hypothesis, we show that the material formulation of the finite theory can be derived following analogous steps to those followed in the infinitesimal case. This is possible due to the fact that the second-order tensor on which depends Ψ_{neq} in Eq. (4), i.e. the non-equilibrated elastic strain tensor \mathbf{A}_e , can be expressed as an explicit function of \mathbf{A} and \mathbf{X}_v , which may both be taken as the independent variables of the continuum formulation

$$\mathbf{A}_e(\mathbf{A}, \mathbf{X}_v) = \mathbf{X}_v^{-T} (\mathbf{A} - \mathbf{A}_v) \mathbf{X}_v^{-1} = \mathbf{X}_v^{-T} \odot \mathbf{X}_v^{-T} : (\mathbf{A} - \mathbf{A}_v) \quad (5)$$

The symbol \odot in the preceding expression denotes the mixed dyadic product between second-order tensors $(\mathbf{Y} \odot \mathbf{Z})_{ijkl} = Y_{ik}Z_{jl}$.

The setting is different for the reversed decomposition given in Eq. (3) because an explicit expression of \mathbf{A}_e in terms of \mathbf{A} and \mathbf{X}_v is not found, so the material formulation cannot be, a priori, derived as made with the original multiplicative decomposition. However, we show next that the material formulation for the reversed decomposition (and analogously, for the Sidoroff's one) can be alternatively derived departing from the spatial formulation. Subsequently, we will be able to develop a model for finite anisotropic visco-hyperelasticity based on the reverse multiplicative decomposition and logarithmic strains following similar conceptual steps to those explained in Ref. [20].

3.1. Spatial description

From the reverse multiplicative decomposition of the deformation gradient $\mathbf{X} = \mathbf{X}_v \mathbf{X}_e$, the expression of the spatial velocity gradient $\mathbf{l} = \dot{\mathbf{X}} \mathbf{X}^{-1}$ in terms of the viscous velocity gradient $\mathbf{l}_v = \dot{\mathbf{X}}_v \mathbf{X}_v^{-1}$ and the elastic velocity gradient $\mathbf{l}_e = \dot{\mathbf{X}}_e \mathbf{X}_e^{-1}$ reads

$$\mathbf{l} = \mathbf{l}_v + \mathbf{X}_v \mathbf{l}_e \mathbf{X}_v^{-1} \quad (6)$$

where \mathbf{l} and \mathbf{l}_v operate in the current configuration and \mathbf{l}_e does in the intermediate configuration. As made in Ref. [20], we are interested herein in obtaining the elastic deformation rate tensor $\mathbf{d}_e = \text{sym}(\mathbf{l}_e)$ as a function of both the deformation rate tensor $\mathbf{d} = \text{sym}(\mathbf{l})$ and the viscous velocity gradient \mathbf{l}_v (or some quantity related to the latter one). From Eq. (6) we obtain in the intermediate configuration

$$\mathbf{d}_e(\mathbf{d}, \mathbf{l}_v^\circ) = \text{sym}(\mathbf{X}_v^{-1} \mathbf{d} \mathbf{X}_v) - \text{sym}(\mathbf{X}_v^{-1} \mathbf{l}_v^\circ \mathbf{X}_v) \quad (7)$$

where \mathbf{l}_v° stands for the co-rotational viscous velocity gradient

$$\mathbf{l}_v^\circ := \mathbf{l}_v - \mathit{skew}(\mathbf{l}) = \mathbf{l}_v - \mathbf{w} = \left(\dot{\mathbf{X}}_v - \mathbf{w} \mathbf{X}_v \right) \mathbf{X}_v^{-1} =: \overset{\circ}{\mathbf{X}}_v \mathbf{X}_v^{-1} \quad (8)$$

and $\overset{\circ}{\mathbf{X}}_v$ for the co-rotational rate of the viscous gradient. Since the co-rotational total velocity gradient is given by $\mathbf{l}^\circ := \mathbf{l} - \mathbf{w} = \mathbf{d}$, note that the two independent variables in rate form in Eq. (7) may be seen as co-rotational (Jaumann-Zaremba) rates, i.e. $\mathbf{d}_e(\mathbf{d}, \mathbf{l}_v^\circ) = \mathbf{d}_e(\mathbf{l}^\circ, \mathbf{l}_v^\circ)$. Equation (7) may be rewritten as

$$\mathbf{d}_e(\mathbf{d}, \mathbf{l}_v^\circ) = \mathbb{M}_d^{d_e} \Big|_{\mathbf{l}_v^\circ = \mathbf{0}} : \mathbf{d} + \mathbb{M}_{\mathbf{l}_v^\circ}^{d_e} \Big|_{\mathbf{d} = \mathbf{0}} : \mathbf{l}_v^\circ \quad (9)$$

where, for further use, we just identify the fourth-order mapping tensor —we omit (minor) symmetrization issues for the matter of notation simplicity

$$\mathbb{M}_d^{d_e} \Big|_{\mathbf{l}_v^\circ = \mathbf{0}} = \frac{1}{2} (\mathbf{X}_v^{-1} \odot \mathbf{X}_v^T + \mathbf{X}_v^T \odot \mathbf{X}_v^{-1}) =: \mathbf{X}_v^{-1} \overset{s}{\odot} \mathbf{X}_v^T \quad (10)$$

This purely geometrical tensor lacks major symmetry in general and is responsible for the lack of symmetry of the global tangent as it will be seen below. Equations (7) or (9) may also be interpreted as

$$\mathbf{d}_e = \mathbf{d}_e(\mathbf{d}, \mathbf{0}) + \mathbf{d}_e(\mathbf{0}, \mathbf{l}_v^\circ) = \mathbf{d}_e \Big|_{\mathbf{l}_v^\circ = \mathbf{0}} + \mathbf{d}_e \Big|_{\mathbf{d} = \mathbf{0}} \quad (11)$$

This interpretation will be useful in the two-step predictor-corrector integration scheme used below. Note that with the consideration of the co-rotational rate of the viscous gradient instead of its total rate, we arrive at a formulation which is conceptually analogous to the spatial formulation based on the Sidoroff's decomposition of Ref. [20]. In this case the virtual state for which $\mathbf{l}_v^\circ = \mathbf{0}$, representing the

state in which the viscous velocity gradient relative to a reference frame with spin \boldsymbol{w} vanishes, naturally emerges from the (reversed) kinematic decomposition given in Eq. (7). This state will define the internal kinematic constraint for no dissipation, as we see below.

The material rate of Eq. (4) yields —we use $d(\cdot)/d(*)$ to denote total differentiation of (\cdot) with respect to the tensorial variable $(*)$

$$\begin{aligned}\dot{\Psi} &= \dot{\Psi}_{eq}(\boldsymbol{A}) + \dot{\Psi}_{neq}(\boldsymbol{A}_e) \\ &= \frac{d\Psi_{eq}}{d\boldsymbol{A}} : \dot{\boldsymbol{A}} + \frac{d\Psi_{neq}}{d\boldsymbol{A}_e} : \dot{\boldsymbol{A}}_e \\ &= \boldsymbol{S}_{eq} : \dot{\boldsymbol{A}} + \boldsymbol{S}_{neq}^{|e} : \dot{\boldsymbol{A}}_e\end{aligned}\tag{12}$$

where the superscript in expressions of the type $(\bullet)^{|e}$ indicates that the variable (\bullet) has been obtained through differentiation with respect to the internal *elastic* strains (\boldsymbol{A}_e in this case). This distinction will show relevant below. Since $\dot{\boldsymbol{A}}_e$ is the pull-back of \boldsymbol{d}_e from the intermediate configuration to the reference configuration by means of

$$\dot{\boldsymbol{A}}_e = \boldsymbol{X}_e^T \boldsymbol{d}_e \boldsymbol{X}_e = \boldsymbol{X}_e^T \odot \boldsymbol{X}_e^T : \boldsymbol{d}_e =: \mathbb{M}_{\boldsymbol{d}_e}^{\dot{\boldsymbol{A}}_e} : \boldsymbol{d}_e\tag{13}$$

and $\dot{\boldsymbol{A}}$ is the pull-back of \boldsymbol{d} from the actual configuration to the reference configuration

$$\dot{\boldsymbol{A}} = \boldsymbol{X}^T \boldsymbol{d} \boldsymbol{X} = \boldsymbol{X}^T \odot \boldsymbol{X}^T : \boldsymbol{d} =: \mathbb{M}_{\boldsymbol{d}}^{\dot{\boldsymbol{A}}} : \boldsymbol{d}\tag{14}$$

the respective push-forward operations of the terms in the right-hand side of Eq.

(12) become

$$\begin{aligned}
\dot{\Psi} &= \mathbf{S}_{eq} : \mathbf{X}^T d\mathbf{X} + \mathbf{S}_{neq}^{|e} : \mathbf{X}_e^T d_e \mathbf{X}_e \\
&= \mathbf{X} \mathbf{S}_{eq} \mathbf{X}^T : d + \mathbf{X}_e \mathbf{S}_{neq}^{|e} \mathbf{X}_e^T : d_e \\
&= \boldsymbol{\tau}_{eq} : d + \boldsymbol{\tau}_{neq}^{|e} : d_e
\end{aligned} \tag{15}$$

In Eq. (15) we have defined the symmetric Kirchhoff stress tensors $\boldsymbol{\tau}_{eq}$ (operating in the actual configuration) and $\boldsymbol{\tau}_{neq}^{|e}$ (operating in the intermediate configuration) as

$$\boldsymbol{\tau}_{eq} := \mathbf{X} \mathbf{S}_{eq} \mathbf{X}^T = \mathbf{S}_{eq} : \mathbf{X}^T \odot \mathbf{X}^T = \mathbf{S}_{eq} : \mathbb{M}_d^A \tag{16}$$

$$\boldsymbol{\tau}_{neq}^{|e} := \mathbf{X}_e \mathbf{S}_{neq}^{|e} \mathbf{X}_e^T = \mathbf{S}_{neq}^{|e} : \mathbf{X}_e^T \odot \mathbf{X}_e^T = \mathbf{S}_{neq}^{|e} : \mathbb{M}_{d_e}^A \tag{17}$$

The insertion of Eq. (9) into Eq. (15) gives

$$\dot{\Psi} = \underbrace{\left(\boldsymbol{\tau}_{eq} + \boldsymbol{\tau}_{neq}^{|e} : \mathbb{M}_d^{d_e} \Big|_{l_v^\circ = \mathbf{0}} \right) : d}_{\dot{\Psi} \Big|_{l_v^\circ = \mathbf{0}}} + \underbrace{\boldsymbol{\tau}_{neq}^{|e} : \mathbb{M}_{l_v^\circ}^{d_e} \Big|_{d=\mathbf{0}} : l_v^\circ}_{\dot{\Psi} \Big|_{d=\mathbf{0}}} \tag{18}$$

where the mapping tensors $\mathbb{M}_d^{d_e} \Big|_{l_v^\circ = \mathbf{0}}$ and $\mathbb{M}_{l_v^\circ}^{d_e} \Big|_{d=\mathbf{0}}$ perform the adequate transformations to the spatial configuration for work-conjugacy.

The dissipation inequality in spatial description

$$\boldsymbol{\tau} : d - \dot{\Psi} = \left(\boldsymbol{\tau} - \boldsymbol{\tau}_{eq} - \boldsymbol{\tau}_{neq}^{|e} : \mathbb{M}_d^{d_e} \Big|_{l_v^\circ = \mathbf{0}} \right) : d - \boldsymbol{\tau}_{neq}^{|e} : \mathbb{M}_{l_v^\circ}^{d_e} \Big|_{d=\mathbf{0}} : l_v^\circ \geq 0 \tag{19}$$

is fulfilled in any case if, first ($l_v^\circ = \mathbf{0}$ implies no dissipation, so the equality must hold)

$$\boldsymbol{\tau} = \boldsymbol{\tau}_{eq} + \boldsymbol{\tau}_{neq}^{|e} : \mathbb{M}_d^{d_e} \Big|_{l_v^\circ = \mathbf{0}} = \boldsymbol{\tau}_{eq} + \boldsymbol{\tau}_{neq} \tag{20}$$

and, second, the Kirchhoff stresses $\boldsymbol{\tau}_{neq}^{|e}$ dissipate power with the pull-back of \boldsymbol{l}_v° from the current configuration to the intermediate one

$$-\boldsymbol{\tau}_{neq}^{|e} : \mathbb{M}_{\boldsymbol{l}_v^\circ}^{d_e} \Big|_{\boldsymbol{d}=\mathbf{0}} : \boldsymbol{l}_v^\circ = \boldsymbol{\tau}_{neq}^{|e} : \boldsymbol{X}_v^{-1} \boldsymbol{l}_v^\circ \boldsymbol{X}_v \geq 0 \quad (21)$$

where Eq. (7) and the symmetry of $\boldsymbol{\tau}_{neq}^{|e}$ have been used. Equation (20) shows that the existing geometrical mapping between the non-equilibrated Kirchhoff stress tensors $\boldsymbol{\tau}_{neq}$, operating in the actual configuration, and $\boldsymbol{\tau}_{neq}^{|e}$, defined in the intermediate configuration, is given by the same mapping tensor that relates \boldsymbol{d} to \boldsymbol{d}_e when $\boldsymbol{l}_v^\circ = \mathbf{0}$, i.e that of Eq. (10) —compare to the original Sidoroff's decomposition where $\boldsymbol{\tau}_{neq} = \boldsymbol{\tau}_{neq}^{|e}$

$$\begin{aligned} \boldsymbol{\tau}_{neq} &= \boldsymbol{\tau}_{neq}^{|e} : \mathbb{M}_d^{d_e} \Big|_{\boldsymbol{l}_v^\circ=\mathbf{0}} = \boldsymbol{\tau}_{neq}^{|e} : \boldsymbol{X}_v^{-1} \overset{s}{\odot} \boldsymbol{X}_v^T \\ &= \frac{1}{2} (\boldsymbol{X}_v^{-T} \boldsymbol{\tau}_{neq}^{|e} \boldsymbol{X}_v^T + \boldsymbol{X}_v \boldsymbol{\tau}_{neq}^{|e} \boldsymbol{X}_v^{-1}) \end{aligned} \quad (22)$$

From the definition of $\boldsymbol{\tau}_{neq}$ in terms of $\boldsymbol{\tau}_{neq}^{|e}$, we notice the equivalence between the following non-dissipative mechanical powers

$$\boldsymbol{\tau}_{neq} : \boldsymbol{d} = \boldsymbol{\tau}_{neq}^{|e} : \boldsymbol{d}_e \Big|_{\boldsymbol{l}_v^\circ=\mathbf{0}} = \dot{\Psi}_{neq} \Big|_{\boldsymbol{l}_v^\circ=\mathbf{0}} \quad (23)$$

Finally, the dissipated power due to viscous effects given in Eq. (21) can be rewritten using Eq. (11) as

$$-\boldsymbol{\tau}_{neq}^{|e} : \mathbb{M}_{\boldsymbol{l}_v^\circ}^{d_e} \Big|_{\boldsymbol{d}=\mathbf{0}} : \boldsymbol{l}_v^\circ = -\boldsymbol{\tau}_{neq}^{|e} : \boldsymbol{d}_e \Big|_{\boldsymbol{d}=\mathbf{0}} \geq 0 \quad (24)$$

which can be read as

$$\dot{\Psi}_{neq} \Big|_{\boldsymbol{d}=\mathbf{0}} \leq 0 \quad (25)$$

The dissipation inequality in spatial description given in Eq. (24) will let us define a general anisotropic constitutive equation for the viscous flow based on material elastic logarithmic strains in the next sections.

3.2. Material description

From Eqs. (9)–(11) we obtain

$$\mathbf{d}_e|_{\mathbf{l}_v^o=\mathbf{0}} = \mathbb{M}_d^{d_e}|_{\mathbf{l}_v^o=\mathbf{0}} : \mathbf{d} \quad (26)$$

Using Eqs. (13) and (14), the Lagrangian counterpart of Eq. (26) is —note that we can equivalently use the subscripts $\mathbf{l}_v^o = \mathbf{0}$ or $\dot{\mathbf{X}}_v = \mathbf{0}$ in order to refer to the same non-dissipative state

$$\dot{\mathbf{A}}_e \Big|_{\dot{\mathbf{X}}_v=\mathbf{0}} = \mathbb{M}_{d_e}^{\dot{\mathbf{A}}_e} : \mathbb{M}_d^{d_e} \Big|_{\mathbf{l}_v^o=\mathbf{0}} : \mathbb{M}_{\dot{\mathbf{A}}}^d : \dot{\mathbf{A}} = \frac{\delta \mathbf{A}_e}{\delta \mathbf{A}} \Big|_{\dot{\mathbf{X}}_v=\mathbf{0}} : \dot{\mathbf{A}} \quad (27)$$

where we define the *modified* partial gradient

$$\begin{aligned} \frac{\delta \mathbf{A}_e}{\delta \mathbf{A}} \Big|_{\dot{\mathbf{X}}_v=\mathbf{0}} &:= \mathbb{M}_{d_e}^{\dot{\mathbf{A}}_e} : \mathbb{M}_d^{d_e} \Big|_{\mathbf{l}_v^o=\mathbf{0}} : \mathbb{M}_{\dot{\mathbf{A}}}^d \\ &= \mathbf{X}_e^T \odot \mathbf{X}_e^T : \mathbf{X}_v^{-1} \overset{s}{\odot} \mathbf{X}_v^T : \mathbf{X}^{-T} \odot \mathbf{X}^{-T} \\ &= \mathbf{C}_e \mathbf{C}^{-1} \overset{s}{\odot} \mathbf{I} \end{aligned} \quad (28)$$

as the fourth-order tensor that maps the strain rate $\dot{\mathbf{A}}$ to the strain rate $\dot{\mathbf{A}}_e$ when there is no dissipation. The same result given in Eq. (28) is obtained taking the time derivative of the elastic right Cauchy-Green deformation tensor \mathbf{C}_e (given in terms of the deformation gradient \mathbf{X} and the left Cauchy-Green deformation tensor $\mathbf{B}_v^{-1} = \mathbf{X}_v^{-T} \mathbf{X}_v^{-1}$ as $\mathbf{C}_e = \mathbf{X}^T \mathbf{B}_v^{-1} \mathbf{X}$) and then specializing the result to the internal state for which $\mathbf{l}_v = \mathbf{w}$. In contrast to the formulation presented in Ref. [20], the

viscous gradient \mathbf{X}_v does not remain completely constant when the mapping tensor given in Eq. (28) is calculated (recall that $\dot{\mathbf{X}}_v = \mathbf{0}$ implies $\dot{\mathbf{X}}_v = \mathbf{w}\mathbf{X}_v$). As a result, that mapping tensor does not correspond in general to the partial gradient of \mathbf{A}_e with respect to \mathbf{A} from a mathematical point of view. This fact will be relevant below. Interestingly, a clear parallelism between the formulations based on the reversed multiplicative decomposition and the Sidoroff's one may be established if we use the symbol δ (instead of ∂) to represent the partial variation of a non-equilibrated variable constrained by $\dot{\mathbf{X}}_v = \mathbf{0}$ (instead of $\dot{\mathbf{X}}_v = \mathbf{0}$). Hereafter we adopt that notation.

Using Eq. (27) we obtain the following equivalent material descriptions of the non-dissipative stress power per unit reference volume —compare to Eq. (23)

$$\mathbf{S}_{neq}^{|e} : \dot{\mathbf{A}}_e \Big|_{\dot{\mathbf{X}}_v = \mathbf{0}} = \mathbf{S}_{neq} : \dot{\mathbf{A}} = \dot{\Psi}_{neq} \Big|_{\dot{\mathbf{X}}_v = \mathbf{0}} \quad (29)$$

This interpretation gives the existing mapping between the non-equilibrated Second Piola-Kirchhoff stress tensors \mathbf{S}_{neq} and $\mathbf{S}_{neq}^{|e}$

$$\mathbf{S}_{neq} = \mathbf{S}_{neq}^{|e} : \frac{\delta \mathbf{A}_e}{\delta \mathbf{A}} \Big|_{\dot{\mathbf{X}}_v = \mathbf{0}} = \frac{d\Psi_{neq}(\mathbf{A}_e)}{d\mathbf{A}_e} : \frac{\delta \mathbf{A}_e}{\delta \mathbf{A}} \Big|_{\dot{\mathbf{X}}_v = \mathbf{0}} = \frac{\delta \Psi_{neq}}{\delta \mathbf{A}} \Big|_{\dot{\mathbf{X}}_v = \mathbf{0}} \quad (30)$$

Both stress tensors \mathbf{S}_{neq} and $\mathbf{S}_{neq}^{|e}$ operate in the reference configuration but they are associated to different deformations, represented by \mathbf{A} and \mathbf{A}_e respectively. Furthermore, Identity (30)₃ provides the way in which the non-equilibrated stresses \mathbf{S}_{neq} are obtained from Ψ_{neq} in this case, i.e. by means of the partial *variation* of Ψ_{neq} with respect to \mathbf{A} along the non-dissipative, corotational path $\dot{\mathbf{X}}_v = \mathbf{0}$.

4. Finite strain viscoelasticity based on logarithmic strain measures

In the preceding section we have obtained all the required tensors needed to properly formulate a finite fully nonlinear visco-hyperelastic model based on the reversed decomposition defined in terms of Green-Lagrange measures. This continuum formulation is valid for anisotropic compressible materials. However, we are mostly interested in formulating a model for nearly-incompressible materials using logarithmic strains because of both their special properties [21] and the possibility of using spline-based stored energy functions [27, 28, 29].

In order to achieve our objective, it is convenient to decompose first the total deformation gradient using the Flory's decomposition

$$\mathbf{X} = (J^{1/3} \mathbf{I}) \mathbf{X}^d \quad (31)$$

where $\det(\mathbf{X}^d) = 1$, and, subsequently, decompose the distortional part of the deformation gradient by means of the reversed decomposition

$$\mathbf{X}^d = \mathbf{X}_v^d \mathbf{X}_e^d \equiv \mathbf{X}_v \mathbf{X}_e \quad (32)$$

That way, the isochoric nature of the non-equilibrium part is exactly preserved by construction.

As it is usual when modelling the mechanical behavior of (nearly-)incompressible materials with application in finite element procedures, Eq. (4) is divided into uncoupled deviatoric and volumetric parts. In terms of the material logarithmic strain measures associated the preceding multiplicative decompositions, it reads

$$\Psi = \mathcal{W} + \mathcal{U} = \mathcal{W}_{eq}(\mathbf{E}^d) + \mathcal{W}_{neq}(\mathbf{E}_e^d) + \mathcal{U}_{eq}(J) \quad (33)$$

where both \mathbf{E} and $\mathbf{E}_e^d \equiv \mathbf{E}_e$ are defined in the reference configuration as

$$\mathbf{E} = \frac{1}{2} \ln(\mathbf{C}) = \frac{1}{2} \ln(\mathbf{X}^T \mathbf{X}) \quad \text{and} \quad \mathbf{E}_e = \frac{1}{2} \ln(\mathbf{C}_e) = \frac{1}{2} \ln(\mathbf{X}_e^T \mathbf{X}_e) \quad (34)$$

with

$$\mathbf{E}^d = \mathbf{E} - \frac{1}{3} \text{tr}(\mathbf{E}) \quad \text{with} \quad \text{tr}(\mathbf{E}) := \ln J := \ln(\det(\mathbf{X})) \quad (35)$$

In Eq. (33), $\mathcal{W} = \mathcal{W}_{eq} + \mathcal{W}_{neq}$ (both \mathcal{W}_{eq} and \mathcal{W}_{neq} to be determined from experimental data) depends on deviatoric, true, behaviors only and $\mathcal{U} = \mathcal{U}_{eq}$ will be used to introduce the required volumetric penalty constraint to the deformation ($J \approx 1$) in the numerical calculations.

In the next sections we derive the expressions of the second Piola-Kirchhoff stress tensor ${}^{t+\Delta t} \mathbf{S}$ and the corresponding tangent moduli ${}^{t+\Delta t} \mathbb{C}$ when the multiplicative decomposition ${}^t \mathbf{X} = {}^t J^{1/3} {}^t \mathbf{X}_v {}^t \mathbf{X}_e$ is known at t and only the deformation gradient ${}^{t+\Delta t} {}_0 \mathbf{X}$ is known at $t + \Delta t$ —for the incremental formulation we use the notation given in Ref. [1]. We first address how to compute the non-equilibrated contribution and then we address the simpler equilibrated one. Finally, the total stresses and tangent moduli are obtained through ${}^{t+\Delta t} \mathbf{S} = {}^{t+\Delta t} \mathbf{S}_{eq} + {}^{t+\Delta t} \mathbf{S}_{neq}$ and ${}^{t+\Delta t} \mathbb{C} = {}^{t+\Delta t} \mathbb{C}_{eq} + {}^{t+\Delta t} \mathbb{C}_{neq}$.

5. Non-equilibrated contribution

5.1. Constitutive equation for the viscous flow

In order to enforce the physical restriction given in Eq. (24)₂ in the logarithmic strain space, we rewrite it attending to the purely kinematic power-conjugacy equivalence between the stress power given by the elastic deformation rate tensor \mathbf{d}_e and

the stress power given by the material rate of the elastic logarithmic strains $\dot{\mathbf{E}}_e$

$$-\dot{\mathcal{W}}_{neq}\Big|_{\mathbf{d}=\mathbf{0}} = -\boldsymbol{\tau}_{neq}^{|e} : \mathbf{d}_e\Big|_{\mathbf{d}=\mathbf{0}} = -\mathbf{T}_{neq}^{|e} : \dot{\mathbf{E}}_e\Big|_{\dot{\mathbf{E}}=\mathbf{0}} = -\dot{\mathcal{W}}_{neq}\Big|_{\dot{\mathbf{E}}=\mathbf{0}} \geq 0 \quad (36)$$

where we define the non-equilibrated purely deviatoric generalized Kirchhoff stresses as

$$\mathbf{T}_{neq}^{|e} := \frac{d\mathcal{W}_{neq}}{d\mathbf{E}_e} = \frac{d\mathcal{W}_{neq}}{d\mathbf{E}_e^d} : \frac{d\mathbf{E}_e^d}{d\mathbf{E}_e} = \frac{d\mathcal{W}_{neq}}{d\mathbf{E}_e^d} : \mathbb{P}^S \quad (37)$$

with $\mathbb{P}^S = \mathbb{I}^S - \frac{1}{3}\mathbf{I} \otimes \mathbf{I}$ being the fourth-order symmetric deviatoric projection tensor, with components in any given basis

$$(\mathbb{P}^S)_{ijkl} = \frac{1}{2}(\delta_{ik}\delta_{jl} + \delta_{il}\delta_{jk}) - \frac{1}{3}\delta_{ij}\delta_{kl} \quad (38)$$

The stress tensor $\mathbf{T}_{neq}^{|e}$ relates to the Kirchhoff stress tensor $\boldsymbol{\tau}_{neq}^{|e}$ through

$$\mathbf{T}_{neq}^{|e} = \boldsymbol{\tau}_{neq}^{|e} : \mathbb{M}_{\dot{\mathbf{E}}_e}^{d_e} \quad (39)$$

where the mapping tensor $\mathbb{M}_{\dot{\mathbf{E}}_e}^{d_e}$ (not needed herein) may be easily obtained in spectral form [20]. Equation (36) is automatically satisfied if we choose the following flow rule

$$-\frac{d\mathbf{E}_e}{dt}\Big|_{\dot{\mathbf{E}}=\mathbf{0}} = \mathbb{V}^{-1} : \mathbf{T}_{neq}^{|e} \quad (40)$$

for a given fourth-order positive-definite viscosity tensor \mathbb{V}^{-1} , whereupon

$$\mathbf{T}_{neq}^{|e} : \mathbb{V}^{-1} : \mathbf{T}_{neq}^{|e} \geq 0 \quad (41)$$

As an important difference with respect to the models based on the Sidoroff decomposition, note that all the entities present in Eqs. (40) and (41) are defined in the

reference configuration.

5.2. Integration of the evolution equation

The non-linear viscous flow rule given in Eq. (40) can be integrated by means of a two-step, elastic predictor/viscous corrector incremental scheme. Within the elastic predictor substep there is no viscous dissipation, so Eq. (24)₁ yields

$${}^{tr}\mathbf{l}_v^\circ = \mathbf{0} \quad \Rightarrow \quad {}^{tr}\mathbf{l}_v = {}^{t+\Delta t}\mathbf{w} \quad \Rightarrow \quad {}^{tr}\dot{\mathbf{X}}_v = {}^{t+\Delta t}\mathbf{w} {}^{tr}\mathbf{X}_v \quad (42)$$

which may be integrated, employing the usual exponential mapping

$${}^{tr}\mathbf{X}_v = \exp\left({}^{t+\Delta t}\mathbf{w}\Delta t\right) {}^t\mathbf{X}_v \quad (43)$$

The tensor $\exp({}^{t+\Delta t}\mathbf{w}\Delta t)$ can be identified after the integration of the equation $\dot{\mathbf{X}} = \mathbf{l}\mathbf{X}$, i.e.

$${}^{t+\Delta t}{}_0\mathbf{X} = \exp\left({}^{t+\Delta t}\mathbf{l}\Delta t\right) {}^t{}_0\mathbf{X} \approx \exp\left({}^{t+\Delta t}\mathbf{d}\Delta t\right) \exp\left({}^{t+\Delta t}\mathbf{w}\Delta t\right) {}^t{}_0\mathbf{X} \quad (44)$$

and then comparing this approximation to the incremental multiplicative decomposition

$${}^{t+\Delta t}{}_0\mathbf{X} = {}^{t+\Delta t}{}_t\mathbf{X} {}^t{}_0\mathbf{X} = {}^{t+\Delta t}{}_t\mathbf{V} {}^{t+\Delta t}{}_t\mathbf{R} {}^t{}_0\mathbf{X} \quad (45)$$

where ${}^{t+\Delta t}{}_t\mathbf{V}$ and ${}^{t+\Delta t}{}_t\mathbf{R}$ are the stretch and rotation tensors from the left polar decomposition of the incremental deformation gradient ${}^{t+\Delta t}{}_t\mathbf{X}$ relating the configurations at t and $t + \Delta t$. Note that, in general, ${}^{t+\Delta t}{}_0\mathbf{V} \neq {}^{t+\Delta t}{}_t\mathbf{V} {}^t{}_0\mathbf{V}$ and ${}^{t+\Delta t}{}_0\mathbf{R} \neq {}^{t+\Delta t}{}_t\mathbf{R} {}^t{}_0\mathbf{R}$, see discussion in Ref. [25]. However, ${}^{t+\Delta t}{}_0J = {}^{t+\Delta t}{}_tJ {}^t{}_0J$. Hence, we can

approximate the incremental distortional deformation by means of

$$\exp({}^{t+\Delta t}\mathbf{d}^d\Delta t) = {}^{t+\Delta t}\mathbf{V}^d \quad \text{and} \quad \exp({}^{t+\Delta t}\mathbf{w}\Delta t) = {}^{t+\Delta t}\mathbf{R} \quad (46)$$

Equations (43) and (46)₂ provide the definition of the isochoric trial state at time $t + \Delta t$ as —the right arrow decoration means “rotated by ${}^{t+\Delta t}\mathbf{R}$ ”

$${}^{tr}\mathbf{X}_v = {}^{t+\Delta t}\mathbf{R}^t {}_0\mathbf{X}_v =: {}_0\underline{\mathbf{X}}_v \quad (47)$$

$${}^{tr}\mathbf{X}_e = {}^{tr}\mathbf{X}_v^{-1} {}^{t+\Delta t}\mathbf{X}^d = ({}_0\underline{\mathbf{X}}_v^{-1} {}^{t+\Delta t}\mathbf{V}^d {}_0\underline{\mathbf{X}}_v) {}_0\mathbf{X}_e = {}^{t+\Delta t}\mathbf{Y}^d {}_0\mathbf{X}_e \quad (48)$$

where all the quantities needed for the calculation of ${}^{tr}\mathbf{X}_v$ and ${}^{tr}\mathbf{X}_e$ are known. Note that trial states are defined in base of Eq. (43) and have different form from usual set-ups based on the Sidoroff decomposition [17, 13, 20] or the Lee decomposition in plasticity [31, 26, 24]. Hence, in this case, we may interpret that the increment of isochoric deformation ${}^{t+\Delta t}\mathbf{V}^d$ is completely applied to the elastic deformation gradient ${}_0\mathbf{X}_e$ within the trial substep by means of the pull-back of ${}^{t+\Delta t}\mathbf{V}^d$ to the intermediate configuration through, see Figure 3.a

$${}^{t+\Delta t}\mathbf{Y}^d := {}_0\underline{\mathbf{X}}_v^{-1} {}^{t+\Delta t}\mathbf{V}^d {}_0\underline{\mathbf{X}}_v \quad (49)$$

A more intuitive interpretation is obtained if we previously rotate the actual configuration at $t + \Delta t$ with ${}^{t+\Delta t}\mathbf{R}^T$ (i.e. if we remove the rotation ${}^{t+\Delta t}\mathbf{R}$ from the two-point total and viscous deformation gradient tensors) as shown in Figure 3.b. In

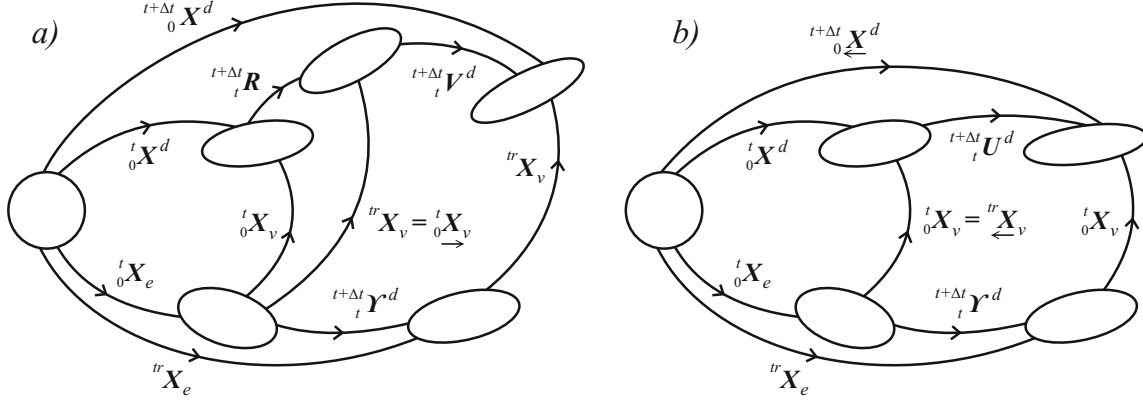


Figure 3: Multiplicative decomposition of the (isochoric) trial state at $t + \Delta t$. Two equivalent interpretations.

that case we have —the left arrow decoration means “rotated by ${}^{t+\Delta t}_t \mathbf{R}^T$ ”

$${}^{t+\Delta t}_0 \overleftarrow{\mathbf{X}}^d := {}^{t+\Delta t}_t \mathbf{R}^T {}^{t+\Delta t}_0 \mathbf{X}^d = {}^{t+\Delta t}_t \mathbf{U}^d {}^t_0 \mathbf{X}^d \quad (50)$$

$$\overleftarrow{tr} \mathbf{X}_v := {}^{t+\Delta t}_t \mathbf{R}^T tr \mathbf{X}_v = {}^t_0 \mathbf{X}_v \quad (51)$$

$$\overleftarrow{tr} \mathbf{X}_e = \overleftarrow{tr} \mathbf{X}_v^{-1} {}^{t+\Delta t}_0 \overleftarrow{\mathbf{X}}^d = ({}^t_0 \mathbf{X}_v^{-1} {}^{t+\Delta t}_t \mathbf{U}^d {}^t_0 \mathbf{X}_v) {}^t_0 \mathbf{X}_e = {}^{t+\Delta t}_t \mathbf{\Upsilon}^d {}^t_0 \mathbf{X}_e \quad (52)$$

where ${}^{t+\Delta t}_t \mathbf{U}^d \approx \exp({}^{t+\Delta t}_t \underline{\mathbf{d}}^d \Delta t)$ is the distortional stretch tensor from the right polar decomposition of ${}^{t+\Delta t}_t \mathbf{X}^d$. Thus we observe that, equivalently, the increment of isochoric deformation ${}^{t+\Delta t}_t \mathbf{U}^d$ is completely applied to the elastic deformation gradient ${}^t_0 \mathbf{X}_e$ within the trial substep by means of the pull-back of ${}^{t+\Delta t}_t \mathbf{U}^d$ to the intermediate configuration through —c.f. Eq.(49)

$${}^{t+\Delta t}_t \mathbf{\Upsilon}^d = {}^t_0 \mathbf{X}_v^{-1} {}^{t+\Delta t}_t \mathbf{U}^d {}^t_0 \mathbf{X}_v \quad (53)$$

In any case, the trial logarithmic strain tensor is

$${}^{tr}\mathbf{E}_e = \frac{1}{2} \ln({}^{tr}\mathbf{C}_e) = \frac{1}{2} \ln({}^{tr}\mathbf{X}_e^T {}^{tr}\mathbf{X}_e) \quad (54)$$

with ${}^{tr}\mathbf{X}_e = \underset{\leftarrow}{\underset{\rightarrow}{t_0}\mathbf{X}_v^{-1} t+\Delta t_0}\mathbf{X}^d$ or ${}^{tr}\mathbf{X}_e = \underset{\leftarrow}{t_0}\mathbf{X}_v^{-1} t+\Delta t_0\mathbf{X}^d$.

Trial states associated to the models based on either the Sidoroff's decomposition or the reversed one are different in general. The respective trial states, and hence the respective integration algorithms, are coincident for the very special cases of axial loadings in isotropic materials or in orthotropic materials along the preferred material directions.

Subsequently, during the viscous corrector substep the total deformation rate $\mathbf{d} = 0$. We exactly proceed as in Ref. [20]

$$\dot{\mathbf{E}} = \mathbf{0} \quad \Rightarrow \quad \dot{\mathbf{E}}_e = \dot{\mathbf{E}}_e \Big|_{\dot{\mathbf{E}}=\mathbf{0}} \quad (55)$$

i.e. using a backward-Euler integration in Eq. (40)

$${}^{t+\Delta t}_0\mathbf{E}_e - {}^{tr}\mathbf{E}_e \approx -\Delta t \left(\mathbb{V}^{-1} : \mathbf{T}_{neq}^{|e} \right)_{t+\Delta t} \quad (56)$$

which provides a non-linear viscous correction for ${}^{t+\Delta t}_0\mathbf{E}_e$ in terms of ${}^{tr}\mathbf{E}_e$ through

$${}^{t+\Delta t}_0\mathbf{E}_e + \Delta t \left(\mathbb{V}^{-1} : \frac{d\mathcal{W}_{neq}}{d\mathbf{E}_e} \right)_{t+\Delta t} = {}^{tr}\mathbf{E}_e \quad (57)$$

The same non-linear evolution equation is obtained for the model based on the Sidoroff's decomposition that we derived in Ref. [20]. In both frameworks, once \mathbb{V}^{-1} and \mathcal{W}_{neq} are known, we can compute ${}^{t+\Delta t}_0\mathbf{E}_e$ for a given time step Δt performing local iterations at the integration point level and then proceed to obtain the deviatoric

non-equilibrated stresses and tangent moduli at $t + \Delta t$. However, two differences of distinct nature have to be emphasized regarding the update of Eq. (57) associated to either the Sidoroff or to the reverse decompositions. On the one hand, we have just seen that the numerical calculation of the trial state is different for both decompositions and that the respective trial states are only coincident in very specific cases. On the other hand, upon the acceptance of the reversed kinematic decomposition, we have seen that Eq. (57) is completely defined in the reference configuration. Hence, no further hypothesis regarding the evolution of the preferred directions are required in this case because the non-equilibrated strain energy function \mathcal{W}_{neq} is defined in the reference configuration and the corresponding Lagrangian non-equilibrated stresses are properly derived in that configuration, whatever the material symmetries are. The tensor \mathbb{V}^{-1} may also be defined with the same material symmetries of \mathcal{W}_{neq} .

For practical purposes but without loss of generality of the present formulation, we will assume herein that \mathbb{V}^{-1} is a purely deviatoric orthotropic tensor given in terms of six scalar viscosity parameters $\eta_{ij}^d = \eta_{ji}^d$ through

$$\mathbb{V}^{-1} = \mathbb{P}^S : \underbrace{\left(\sum_{i=1}^3 \sum_{j=1}^3 \frac{1}{2\eta_{ij}^d} \mathbf{L}_{ij}^S \otimes \mathbf{L}_{ij}^S \right)}_{\bar{\mathbb{V}}^{-1}} : \mathbb{P}^S \quad (58)$$

where $\mathbf{L}_{ij}^S = 1/2(\mathbf{a}_i \otimes \mathbf{a}_j + \mathbf{a}_j \otimes \mathbf{a}_i)$ stand for the structural tensors associated to the material preferred basis $X_{pr} = \{\mathbf{a}_1, \mathbf{a}_2, \mathbf{a}_3\}$. The evolution equation in rate form Eq. (40) and its solution in terms of incremental elastic strains Eq. (57) become purely deviatoric. It is apparent that, in general, ${}^{t+\Delta t}_0 \mathbf{E}_e$ and ${}^{tr} \mathbf{E}_e$ in Eq. (57) will not have the same Lagrangian principal basis. In Section 7 we show how to obtain the values of the material parameters η_{ij}^d from experimental testing. Once the viscosity

parameters η_{ij}^d are known, the non-linear Equations (40) and (57) are to be used. In those equations we will further assume that the viscosity parameters are deformation independent.

The value of the material parameters η_{ij}^d in Eq. (58) may be related to a set of six independent relaxation times $\tau_{ij} = \tau_{ji}$ for the orthotropic case. Note that we use the same symbol for the relaxation times as for the Kirchhoff stresses but by context confusion is hardly possible.

In order to obtain the existing relations between η_{ij}^d and τ_{ij} we must linearize the response of the non-equilibrated orthotropic strain energy function \mathcal{W}_{neq} in the flow rule of Eq. (40) to obtain

$$-\left. \frac{d\mathbf{E}_e}{dt} \right|_{\dot{\mathbf{E}}=0} = \mathbb{P}^S : \underbrace{\left(\bar{\mathbb{V}}^{-1} : \mathbb{P}^S : \left. \frac{d^2 \mathcal{W}_{neq}}{d\mathbf{E}_e^d d\mathbf{E}_e^d} \right|_{lin} \right)}_{\bar{\mathbb{T}}_{lin}^{-1}} : \mathbb{P}^S : \mathbf{E}_e = \mathbb{T}_d^{-1} \Big|_{lin} : \mathbf{E}_e \quad (59)$$

where

$$\mathcal{W}_{neq}(\mathbf{E}_e^d) \Big|_{lin} = \sum_{i=1}^3 \sum_{j=1}^3 \mu_{ij}^{neq} (\mathbf{a}_i \cdot \mathbf{E}_e^d \mathbf{a}_j)^2 = \sum_{i=1}^3 \sum_{j=1}^3 \mu_{ij}^{neq} (E_{eij}^d)^2 \quad (60)$$

is expressed in terms of the orthotropic reference shear moduli μ_{ij}^{neq} and the components of \mathbf{E}_e^d in the material orthotropy basis $X_{pr} = \{\mathbf{a}_1, \mathbf{a}_2, \mathbf{a}_3\}$. The subscript *lin* implies a linearized constitutive law (usually at the origin), i.e. quadratic strain energy with constant coefficients. The linearized fourth-order deviatoric *relaxation* tensor $\mathbb{T}_d^{-1} \Big|_{lin}$ present in Eq. (59) is given in terms of the tensor $\bar{\mathbb{T}}_{lin}^{-1}$, whose matrix

(Voigt) representation in the preferred axes X_{pr} is

$$[\bar{\mathbb{T}}_{lin}^{-1}]_{X_{pr}} = \begin{bmatrix} \frac{2}{3} \frac{1}{\tau_{11}} & -\frac{1}{3} \frac{\rho_{21}}{\tau_{22}} & -\frac{1}{3} \frac{\rho_{31}}{\tau_{33}} & 0 & 0 & 0 \\ -\frac{1}{3} \frac{\rho_{12}}{\tau_{11}} & \frac{2}{3} \frac{1}{\tau_{22}} & -\frac{1}{3} \frac{\rho_{32}}{\tau_{33}} & 0 & 0 & 0 \\ -\frac{1}{3} \frac{\rho_{13}}{\tau_{11}} & -\frac{1}{3} \frac{\rho_{23}}{\tau_{22}} & \frac{2}{3} \frac{1}{\tau_{33}} & 0 & 0 & 0 \\ 0 & 0 & 0 & \frac{1}{\tau_{12}} & 0 & 0 \\ 0 & 0 & 0 & 0 & \frac{1}{\tau_{23}} & 0 \\ 0 & 0 & 0 & 0 & 0 & \frac{1}{\tau_{31}} \end{bmatrix} \quad (61)$$

The relaxation times τ_{ij} and the coupling coefficients ρ_{ij} are given by

$$\tau_{ij} := \frac{\eta_{ij}^d}{\mu_{ij}^{neq}}, \quad i, j = \{1, 2, 3\} \quad (62)$$

$$\rho_{ij} := \frac{\eta_{ii}^d}{\eta_{jj}^d}, \quad i \neq j = \{1, 2, 3\} \quad (63)$$

The tensor $\bar{\mathbb{T}}_{lin}^{-1}$, as given in Eq. (61), is non-symmetric in general. We remark that, as a main difference with the isotropic viscosity/orthotropic elasticity formulation presented in Ref. [20], the six relaxation times given in Eq. (62) are completely independent, hence leading to a more general anisotropic visco-hyperelasticity formulation. We show the high (enhanced) versatility of the present model in the examples below. If the viscosity tensor is regarded as isotropic in Eq. (58), then we can write $\mathbb{V}^{-1} = 1/(2\eta^d)\mathbb{I}^S$ and the update formula Eq. (57) adopts the same form as in Ref. [20], even though it is formulated herein in the reference configuration. Equation (61) reduces in this case to $\bar{\mathbb{T}}_{lin}^{-1} = \mathbb{P}^S : \mathbb{T}_{lin}^{-1}$, with \mathbb{T}_{lin}^{-1} resulting in a tensor with diagonal matrix representation, which was for simplicity the shape chosen in

Reference [20] for isotropic viscous behavior.

Finally, once a converged solution ${}^{t+\Delta t}_0 \mathbf{E}_e$ has been obtained from Eq. (57), the following (internal volume-preserving) update may be performed

$${}^{t+\Delta t}_0 \mathbf{X}_e = {}^{tr} \mathbf{R}_e {}^{t+\Delta t}_0 \mathbf{U}_e = {}^{tr} \mathbf{R}_e \exp \left({}^{t+\Delta t}_0 \mathbf{E}_e \right) \quad (64)$$

or

$${}^{t+\Delta t}_0 \mathbf{X}_v = {}^{t+\Delta t}_0 \mathbf{X}^d {}^{t+\Delta t}_0 \mathbf{X}_e^{-1} = {}^{tr} \mathbf{X}_v \left({}^{tr} \mathbf{V}_e {}^{t+\Delta t}_0 \mathbf{V}_e^{-1} \right) \quad (65)$$

5.3. Local Newton iterations for the non-equilibrated part

Once the trial elastic logarithmic strains ${}^{tr} \mathbf{E}_e$ have been obtained using Eq. (54), we proceed to solve Eq. (57) in residual form for the most general case when hyperelasticity is non-linear in logarithmic strains. We can proceed as in Ref. [20] but considering the residual equation

$$\mathbf{R}_E^{(k)} = \mathbf{E}_e^{(k)} + \Delta t \left(\mathbb{V}^{-1} : \frac{d\mathcal{W}_{neq}}{d\mathbf{E}_e} \Big|_{(k)} \right) - {}^{tr} \mathbf{E}_e \quad (66)$$

and employing the *non-symmetric* gradient

$$\frac{d\mathbf{R}_E}{d\mathbf{E}_e} = \mathbb{I}^S + \Delta t \left(\mathbb{V}^{-1} : \frac{d^2 \mathcal{W}_{neq}}{d\mathbf{E}_e d\mathbf{E}_e} \right) = \mathbb{I}^S + \mathbb{P}^S : \Delta t \left(\bar{\mathbb{V}}^{-1} : \mathbb{P}^S : \frac{d^2 \mathcal{W}_{neq}}{d\mathbf{E}_e^d d\mathbf{E}_e^d} \right) : \mathbb{P}^S \quad (67)$$

The resulting iterative procedure for \mathbf{E}_e is volume-preserving due to the fact that the term between parenthesis in Eq. (66) is purely deviatoric.

5.4. Non-equilibrated contribution to \mathbf{S} and \mathbb{C}

Once the elastic strains \mathbf{E}_e are known at $t + \Delta t$ we can proceed to compute the deviatoric non-equilibrated contribution to the stress and global tangent tensors. As

we did in Ref. [20], it is convenient to take derivatives with respect to trial quantities in order to obtain the non-equilibrated stresses and tangent moduli consistent with the predictor/corrector integration algorithm employed and then perform the corresponding mappings.

First of all, the consideration of the Flory's decomposition of Eq. (31) in Eq. (30)₃ gives

$$\mathbf{S}_{neq} = \frac{\delta \mathcal{W}_{neq}}{\delta \mathbf{A}} \Big|_{\dot{\mathbf{X}}_v=0} = \frac{\delta \mathcal{W}_{neq}}{\delta \mathbf{A}^d} \Big|_{\dot{\mathbf{X}}_v=0} : \frac{d\mathbf{A}^d}{d\mathbf{A}} := \mathbf{S}_{neq}^{|d} : \frac{d\mathbf{A}^d}{d\mathbf{A}} \quad (68)$$

where $\mathbf{S}_{neq}^{|d}$ is a modified second Piola–Kirchhoff stress tensor defined in the reference configuration and $d\mathbf{A}^d/d\mathbf{A}$ represents the fourth-order deviatoric projection tensor in the space of quadratic strains, see below.

The trial state is defined by ${}^{tr}\mathbf{l}_v^\circ = \mathbf{0}$. Then the distortional counterpart of Eqs. (7), (9) and (10) particularized to the trial state read —note that subscripts of the type ${}^{tr}\mathbf{l}_v^\circ = \mathbf{0}$ or ${}^{tr}\dot{\mathbf{X}}_v = \mathbf{0}$ would be redundant for the trial state, hence they are not indicated in the corresponding mapping tensors

$${}^{tr}\mathbf{d}_e = \text{sym} \left({}^{tr}\mathbf{X}_v^{-1} \mathbf{d}^d {}^{tr}\mathbf{X}_v \right) = {}^{tr}\mathbf{X}_v^{-1} \overset{s}{\odot} {}^{tr}\mathbf{X}_v^T : \mathbf{d}^d = \mathbb{M}_{d^d}^{tr d_e} : \mathbf{d}^d \quad (69)$$

As done in Section 3.2, the Lagrangian description of Eq. (69) is obtained as

$${}^{tr}\dot{\mathbf{A}}_e = {}^{tr}\mathbf{C}_e \mathbf{C}^{d-1} \overset{s}{\odot} \mathbf{I} : \dot{\mathbf{A}}^d = \frac{\delta {}^{tr}\mathbf{A}_e}{\delta \mathbf{A}^d} : \dot{\mathbf{A}}^d \quad (70)$$

which gives the mapping associated to the change of the independent variable \mathbf{A}^d by the independent variable ${}^{tr}\mathbf{A}_e$. We define now the non-equilibrated second Piola–Kirchhoff stress tensor $\mathbf{S}_{neq}^{|tr}$ associated to the trial state, which operates in the ref-

erence configuration as well, such that —recall also Eq. (29)

$$\mathbf{S}_{neq}^{|tr} : {}^{tr}\dot{\mathbf{A}}_e = \mathbf{S}_{neq}^{|d} : \dot{\mathbf{A}}^d = \mathbf{S}_{neq} : \dot{\mathbf{A}} = \dot{\mathcal{W}}_{neq} \Big|_{\dot{\mathbf{x}}_v=0} \quad (71)$$

which gives the following relation between the non-equilibrated stress tensors $\mathbf{S}_{neq}^{|d}$ and $\mathbf{S}_{neq}^{|tr}$

$$\mathbf{S}_{neq}^{|d} = \mathbf{S}_{neq}^{|tr} : {}^{tr}\mathbf{C}_e \mathbf{C}^{d-1} \overset{s}{\odot} \mathbf{I} = \mathbf{S}_{neq}^{|tr} : \frac{\delta {}^{tr}\mathbf{A}_e}{\delta \mathbf{A}^d} \quad (72)$$

One important difference between this algorithmic formulation and the one presented in Ref. [20] is that in this case the trial intermediate configuration does not remain constant during the finite-element global iterations at time $t + \Delta t$ because this configuration is given by the trial elastic internal gradient, see Eqs. (48) or (52). Hence, the fourth-order mapping tensor $\delta {}^{tr}\mathbf{A}_e / \delta \mathbf{A}^d$ present in Eq. (72) has also to be differentiated in order to obtain the existing relation between the consistent tangent moduli $\mathbb{C}_{neq}^{|d} = d\mathbf{S}_{neq}^{|d} / d\mathbf{A}^d$ and $\mathbb{C}_{neq}^{|tr} = d\mathbf{S}_{neq}^{|tr} / d{}^{tr}\mathbf{A}_e$, which are to be obtained taking the total derivatives of $\mathbf{S}_{neq}^{|d}$ and $\mathbf{S}_{neq}^{|tr}$ with respect to \mathbf{A}^d and ${}^{tr}\mathbf{A}_e$ respectively, see discussion in Ref. [20]. In this case we have —note that $\delta {}^{tr}\mathbf{A}_e / \delta \mathbf{A}^d$ has only minor symmetries and that the second addend in the right-hand side of the following equation vanishes in the model based on the Sidoroff decomposition

$$\frac{d\mathbf{S}_{neq}^{|d}}{dt} = \frac{d\mathbf{S}_{neq}^{|tr}}{dt} : \frac{\delta {}^{tr}\mathbf{A}_e}{\delta \mathbf{A}^d} + \mathbf{S}_{neq}^{|tr} : \frac{d}{dt} \left(\frac{\delta {}^{tr}\mathbf{A}_e}{\delta \mathbf{A}^d} \right) \quad (73)$$

Expressing the preceding equation in terms of $\dot{\mathbf{A}}^d$ and ${}^{tr}\dot{\mathbf{A}}_e$, using Eq. (70) and identifying terms

$$\frac{d\mathbf{S}_{neq}^{|d}}{d\mathbf{A}^d} = \left(\frac{\delta {}^{tr}\mathbf{A}_e}{\delta \mathbf{A}^d} \right)^T : \frac{d\mathbf{S}_{neq}^{|tr}}{d{}^{tr}\mathbf{A}_e} : \frac{\delta {}^{tr}\mathbf{A}_e}{\delta \mathbf{A}^d} + \mathbf{S}_{neq}^{|tr} : \frac{d}{d\mathbf{A}^d} \left(\frac{\delta {}^{tr}\mathbf{A}_e}{\delta \mathbf{A}^d} \right) \quad (74)$$

which, after some lengthy algebra, results in

$$\begin{aligned} \mathbb{C}_{neq}^{|d} &= \left(\frac{\delta {}^{tr} \mathbf{A}_e}{\delta \mathbf{A}^d} \right)^T : \mathbb{C}_{neq}^{|tr} : \frac{\delta {}^{tr} \mathbf{A}_e}{\delta \mathbf{A}^d} \\ &+ \mathbf{C}^{d-1} {}^{tr} \mathbf{C}_e \mathbf{C}^{d-1} \overset{s}{\odot} \mathbf{S}_{neq}^{|tr} - \mathbf{C}^{d-1} \overset{s}{\odot} \mathbf{S}_{neq}^{|tr} {}^{tr} \mathbf{C}_e \mathbf{C}^{d-1} \end{aligned} \quad (75)$$

The first and second addends in the right-hand side of Eq. (75) have major symmetries, the former due to the major symmetry of $\mathbb{C}_{neq}^{|tr}$ (see below) and the latter due to the symmetry of the second order tensors $\mathbf{C}^{d-1} {}^{tr} \mathbf{C}_e \mathbf{C}^{d-1}$ and $\mathbf{S}_{neq}^{|tr}$. However, the third addend in the right-hand side of Eq. (75) lacks major symmetry, in general. As a result, the tangent moduli tensor $\mathbb{C}_{neq}^{|d}$ may be slightly non-symmetric, as we show in the examples. The lack of major symmetry in general situations emerges from the fact that the fourth-order tensor $\delta {}^{tr} \mathbf{A}_e / \delta \mathbf{A}^d$ present in Eq. (74) does not exactly correspond to the gradient of ${}^{tr} \mathbf{A}_e$ with respect to \mathbf{A}^d , as we have equivalently explained in Section 3.2 using the strain tensors \mathbf{A}_e and \mathbf{A} and the constraint $\dot{\mathbf{X}}_v = \mathbf{0}$, recall also Eq. (10). In other words, note that an explicit expression that gives ${}^{tr} \mathbf{A}_e$ as a function of \mathbf{A}^d does not exist for this formulation in general. However, we want to emphasize that the non-equilibrated strain energy function \mathcal{W}_{neq} only represents a deviation from the thermodynamical equilibrium, hence the possible nonsymmetry of $\mathbb{C}_{neq}^{|d}$ becomes less relevant if the symmetry of the total tangent moduli $\mathbb{C} = \mathbb{C}_{eq} + \mathbb{C}_{neq}$ is assessed. It can be shown that the total tangent moduli \mathbb{C} results to be numerically symmetric for the special case of isotropic materials undergoing large shear deformations (first example below) and exactly symmetric for the special case of orthotropic materials undergoing finite deformations along the preferred material directions (second example below). Furthermore, for orthotropic materials undergoing large off-axis deformations and large perturbations away from

thermodynamical equilibrium, a very good convergence rate is still attained during the global finite element iterations using the symmetric part of Eq. (75) and a symmetric solver (third example below). In order to symmetrize the tensor $\mathbb{C}_{neq}^{|d}$ of Eq. (75), just substitute $\mathbf{S}_{neq}^{|tr} {}^{tr}\mathbf{C}_e \mathbf{C}^{d-1}$ by its symmetric part, i.e. $\mathbf{S}_{neq}^{|d}$, see Eq. (72).

The trial tensors $\mathbf{S}_{neq}^{|tr}$ and $\mathbb{C}_{neq}^{|tr}$, present in Eqs. (72) and (75), may be obtained from our model, based on logarithmic strains, through

$$\mathbf{S}_{neq}^{|tr} = \left. \frac{\delta \mathcal{W}_{neq}}{\delta {}^{tr}\mathbf{A}_e} \right|_{\dot{\mathbf{x}}_v=0} = \left. \frac{\delta \mathcal{W}_{neq}}{\delta {}^{tr}\mathbf{E}_e} \right|_{\dot{\mathbf{x}}_v=0} : \frac{d {}^{tr}\mathbf{E}_e}{d {}^{tr}\mathbf{A}_e} =: \mathbf{T}_{neq}^{|tr} : \frac{d {}^{tr}\mathbf{E}_e}{d {}^{tr}\mathbf{A}_e} \quad (76)$$

and —note that $d {}^{tr}\mathbf{E}_e / d {}^{tr}\mathbf{A}_e$ has major and minor symmetries and that it represents a formal (total) gradient

$$\mathbb{C}_{neq}^{|tr} = \frac{d \mathbf{S}_{neq}^{|tr}}{d {}^{tr}\mathbf{A}_e} = \frac{d {}^{tr}\mathbf{E}_e}{d {}^{tr}\mathbf{A}_e} : \frac{d \mathbf{T}_{neq}^{|tr}}{d {}^{tr}\mathbf{E}_e} : \frac{d {}^{tr}\mathbf{E}_e}{d {}^{tr}\mathbf{A}_e} + \mathbf{T}_{neq}^{|tr} : \frac{d^2 {}^{tr}\mathbf{E}_e}{d {}^{tr}\mathbf{A}_e d {}^{tr}\mathbf{A}_e} \quad (77)$$

The trial generalized Kirchhoff stress tensor $\mathbf{T}_{neq}^{|tr}$ has to be previously related to the updated generalized Kirchhoff stress tensor $\mathbf{T}_{neq}^{|e}$, which is the resulting stress tensor at each global iteration obtained from $\mathcal{W}_{neq}(\mathbf{E}_e^d)$ using Eq. (37). We have —compare to Eq. (30) and consider the change of variable \mathbf{E} by ${}^{tr}\mathbf{E}_e$

$$\mathbf{T}_{neq}^{|tr} = \left. \frac{\delta \mathcal{W}_{neq}}{\delta {}^{tr}\mathbf{E}_e} \right|_{\dot{\mathbf{x}}_v=0} = \frac{d \mathcal{W}_{neq}}{d \mathbf{E}_e} : \left. \frac{\delta \mathbf{E}_e}{\delta {}^{tr}\mathbf{E}_e} \right|_{\dot{\mathbf{x}}_v=0} = \mathbf{T}_{neq}^{|e} : \left. \frac{\delta \mathbf{E}_e}{\delta {}^{tr}\mathbf{E}_e} \right|_{\dot{\mathbf{x}}_v=0} \quad (78)$$

Hereafter, analogously as we did in Ref. [20], we approximate

$$\left. \frac{\delta \mathbf{E}_e}{\delta {}^{tr}\mathbf{E}_e} \right|_{\dot{\mathbf{x}}_v=0} \approx \mathbb{I}^S \quad \Rightarrow \quad \mathbf{T}_{neq}^{|tr} \approx \mathbf{T}_{neq}^{|e} \quad (79)$$

which is an approximation valid for $\Delta t / \tau \ll 1$ in the most general case (as for the model based on the Sidoroff decomposition, note that $\mathbf{T}_{neq}^{|tr} = \mathbf{T}_{neq}^{|e}$ for the special

cases of isotropic materials under arbitrary loadings or orthotropic materials undergoing finite deformations along the preferred material directions). If we do not wish to take this approximation, we should compute the analytical mapping tensor present in Eq. (78) and its derivatives in the numerical algorithm, cf. Ref. [20], Appendix 2. The modified second Piola–Kirchhoff stresses $\mathbf{S}_{neq}^{|d}$ are obtained combining, first, Eqs. (76), (78) and (79)₁

$$\mathbf{S}_{neq}^{|tr} = \left. \frac{d\mathcal{W}_{neq}}{d\mathbf{E}_e} \right|_{t+\Delta t} : \frac{d{}^{tr}\mathbf{E}_e}{d{}^{tr}\mathbf{A}_e} \quad (80)$$

and then performing the mapping from the internal (trial) to the external (isochoric) configurations using Eq. (72).

In order to obtain the consistent tangent moduli $d\mathbf{T}_{neq}^{|tr}/d{}^{tr}\mathbf{E}_e$, needed in Eq. (77), we have to take into consideration that the trial logarithmic strains ${}^{tr}\mathbf{E}_e$ and the updated logarithmic strains ${}^{t+\Delta t}_0\mathbf{E}_e$ are related in the algorithm through Eq. (57). Hence

$$\frac{d\mathbf{T}_{neq}^{|tr}}{d{}^{tr}\mathbf{E}_e} = \frac{d\mathbf{T}_{neq}^{|e}}{d{}^{tr}\mathbf{E}_e} = \frac{d\mathbf{T}_{neq}^{|e}}{d\mathbf{E}_e} : \frac{d{}^{t+\Delta t}_0\mathbf{E}_e}{d{}^{tr}\mathbf{E}_e} \quad (81)$$

with the tensor $d{}^{t+\Delta t}_0\mathbf{E}_e/d{}^{tr}\mathbf{E}_e$ providing the consistent linearization of the algorithmic formulation during the viscous correction substep. Taking derivatives in Eq. (57), we identify

$$\frac{d\mathbf{T}_{neq}^{|tr}}{d{}^{tr}\mathbf{E}_e} = \left. \frac{d^2\mathcal{W}_{neq}}{d\mathbf{E}_e d\mathbf{E}_e} \right|_{t+\Delta t} : \left. \frac{d\mathbf{R}_{\mathbf{E}}}{d\mathbf{E}_e} \right|_{t+\Delta t}^{-1} \quad (82)$$

where the algorithmic gradient $d{}^{t+\Delta t}_0\mathbf{E}_e/d{}^{tr}\mathbf{E}_e$ is given by the inverse of Eq. (67) evaluated at the updated strains ${}^{t+\Delta t}_0\mathbf{E}_e$, see Section 5.3. Note that only the deviatoric part of this tensor is relevant in Eq. (82). Interestingly, although the algorithmic gradient $d{}^{t+\Delta t}_0\mathbf{E}_e/d{}^{tr}\mathbf{E}_e$ is, in general, non-symmetric in this case, the trial consistent tangent tensor $d\mathbf{T}_{neq}^{|tr}/d{}^{tr}\mathbf{E}_e$, as given in Eqs. (81) or (82), has major and

minor symmetries. This is thanks to the fact that the viscosity tensor \mathbb{V}^{-1} in Eq. (40) is fully symmetric [13, 20]. The modified consistent (non-symmetric, in general) tangent moduli $\mathbb{C}_{neq}^{|d}$ for the non-equilibrated part is obtained combining, first, Eqs. (77), (79)₂ and (82) —note that $\mathbb{C}_{neq}^{|tr}$ preserves major and minor symmetries

$$\begin{aligned} \mathbb{C}_{neq}^{|tr} &= \frac{d^{tr} \mathbf{E}_e}{d^{tr} \mathbf{A}_e} : \frac{d^2 \mathcal{W}_{neq}}{d\mathbf{E}_e d\mathbf{E}_e} \Big|_{t+\Delta t} : \frac{d^{t+\Delta t} \mathbf{E}_e}{d^{tr} \mathbf{E}_e} : \frac{d^{tr} \mathbf{E}_e}{d^{tr} \mathbf{A}_e} \\ &+ \frac{d\mathcal{W}_{neq}}{d\mathbf{E}_e} \Big|_{t+\Delta t} : \frac{d^2{}^{tr} \mathbf{E}_e}{d^{tr} \mathbf{A}_e d^{tr} \mathbf{A}_e} \end{aligned} \quad (83)$$

and then mapping the result from the internal to the external configurations using Eq. (75). Mapping tensors relating material logarithmic strains to Green–Lagrange strains are given in spectral form in, for example, Ref. [29], Section 2.5.

Finally, the isochoric non-equilibrated stresses \mathbf{S}_{neq} and consistent tangent moduli $\mathbb{C}_{neq} = d\mathbf{S}_{neq}/d\mathbf{A}$ are obtained from $\mathbf{S}_{neq}^{|d}$ and $\mathbb{C}_{neq}^{|d} = d\mathbf{S}_{neq}^{|d}/d\mathbf{A}^d$ using the deviatoric projection tensor $d\mathbf{A}^d/d\mathbf{A}$ (recall Eq. (68)) and its derivatives through —see Ref. [20], Appendix 1

$$\mathbf{S}_{neq} = J^{-2/3} \mathbf{S}_{neq}^{|d} \quad (84)$$

and

$$\mathbb{C}_{neq} = J^{-4/3} \mathbb{C}_{neq}^{|d} \quad (85)$$

In the derivation of Eq. (85) we have used the fact that the second and third addends in the right-hand side of Eq. (75) cancel to each other when the two-index contraction operations $\mathbf{C}^d : \mathbb{C}_{neq}^{|d}$ and $\mathbb{C}_{neq}^{|d} : \mathbf{C}^d$ are performed, which allows us to consider the symmetry relation $\mathbf{C}^d : \mathbb{C}_{neq}^{|d} = \mathbb{C}_{neq}^{|d} : \mathbf{C}^d$.

5.5. Linearized case: Finite linear viscoelasticity

The constitutive equation for the viscous flow Eq. (40) may be simplified when either linear finite logarithmic or linear small stress-strain relations are derived from the non-equilibrated contribution \mathcal{W}_{neq} . In both cases, the same linear/linearized solution for the evolution equation is obtained, i.e. the so-called Finite Linear Viscoelasticity. The (linear) viscous flow rule for the fully orthotropic model using the reverse multiplicative decomposition represents a generalization of the expression derived for the Sidoroff's decomposition —c.f. Ref. [20]

$$-\left. \frac{d\mathbf{E}_e}{dt} \right|_{\dot{\mathbf{E}}=0} = \mathbb{P}^S : \left(\bar{\mathbb{V}}^{-1} : \mathbb{P}^S : \frac{d^2 \mathcal{W}_{neq}}{d\mathbf{E}_e^d d\mathbf{E}_e^d} \right) : \mathbb{P}^S : \mathbf{E}_e = \mathbb{T}_d^{-1} : \mathbf{E}_e \quad (86)$$

where \mathbf{E}_e is used in this section to represent either the internal elastic logarithmic strain tensor or the internal elastic infinitesimal strains tensor $\boldsymbol{\varepsilon}_e$. The simplification in this case emerges from the fact that the integration of Eq. (86) during the viscous corrector substep gives an explicit update for ${}^{t+\Delta t}_0 \mathbf{E}_e$ in terms of ${}^{tr} \mathbf{E}_e$, i.e. —compare to Eq. (57) for the fully non-linear case

$$\left(\mathbb{I}^S + \Delta t \mathbb{T}_d^{-1} \right) : {}^{t+\Delta t}_0 \mathbf{E}_e = {}^{tr} \mathbf{E}_e \quad \Rightarrow \quad {}^{t+\Delta t}_0 \mathbf{E}_e = \left(\mathbb{I}^S + \Delta t \mathbb{T}_d^{-1} \right)^{-1} : {}^{tr} \mathbf{E}_e \quad (87)$$

so no local Newton iterations are needed.

6. Equilibrated contribution

If the total gradient ${}^{t+\Delta t}_0 \mathbf{X}$ is known at time step $t + \Delta t$, then the equilibrated contributions ${}^{t+\Delta t} \mathbf{S}_{eq}$ and ${}^{t+\Delta t} \mathbb{C}_{eq}$ are just obtained from $\Psi_{eq}(\mathbf{E}) = \mathcal{W}_{eq}(\mathbf{E}^d) + \mathcal{U}_{eq}(J)$ as usual uncoupled deviatoric-volumetric hyperelastic calculations, i.e.

$$\mathbf{S}_{eq} = \frac{d\Psi_{eq}}{d\mathbf{A}} = \frac{d\Psi_{eq}}{d\mathbf{E}} : \frac{d\mathbf{E}}{d\mathbf{A}} = \mathbf{T}_{eq} : \frac{d\mathbf{E}}{d\mathbf{A}} \quad (88)$$

$$\mathbb{C}_{eq} = \frac{d\mathbf{S}_{eq}}{d\mathbf{A}} = \frac{d\mathbf{E}}{d\mathbf{A}} : \frac{d\mathbf{T}_{eq}}{d\mathbf{E}} : \frac{d\mathbf{E}}{d\mathbf{A}} + \mathbf{T}_{eq} : \frac{d^2\mathbf{E}}{d\mathbf{A}d\mathbf{A}} \quad (89)$$

For detailed formulae to compute these contributions for an incompressible orthotropic material, we refer to Ref. [29], Section 2.5.

7. Determination of the viscosity parameters of the orthotropic model

Consider a small strains uniaxial relaxation test performed about the preferred material direction \mathbf{e}_1 of an incompressible material. Equation (59) represented in preferred material axes and specialized at $t = 0^+$ (just after the total deformation in direction \mathbf{e}_1 is applied and retained) reads —note that shear terms are not needed and that $\boldsymbol{\varepsilon}_e^0 = \boldsymbol{\varepsilon}_e(t = 0^+) = \boldsymbol{\varepsilon}(t = 0^+) = \boldsymbol{\varepsilon}^0$ are isochoric (traceless)

$$- \left[\begin{array}{c} \dot{\varepsilon}_{e11}^0 \\ \dot{\varepsilon}_{e22}^0 \\ \dot{\varepsilon}_{e33}^0 \end{array} \right]_{\dot{\varepsilon}=0} = \frac{\varepsilon_{11}^0}{9} \left[\begin{array}{ccc} 2\frac{E_{11}^{neq}}{\eta_{11}^d} + \frac{H_{12}^{neq}}{\eta_{22}^d} + \frac{H_{13}^{neq}}{\eta_{33}^d} \\ -\frac{E_{11}^{neq}}{\eta_{11}^d} - 2\frac{H_{12}^{neq}}{\eta_{22}^d} + \frac{H_{13}^{neq}}{\eta_{33}^d} \\ -\frac{E_{11}^{neq}}{\eta_{11}^d} + \frac{H_{12}^{neq}}{\eta_{22}^d} - 2\frac{H_{13}^{neq}}{\eta_{33}^d} \end{array} \right] \quad (90)$$

where we have defined

$$\begin{aligned} E_{11}^{neq} &:= 2\mu_{11}^{neq} + \mu_{22}^{neq}\nu_{12}^0 + \mu_{33}^{neq}\nu_{13}^0 \\ H_{12}^{neq} &:= \mu_{11}^{neq} + 2\mu_{22}^{neq}\nu_{12}^0 - \mu_{33}^{neq}\nu_{13}^0 \\ H_{13}^{neq} &:= \mu_{11}^{neq} - \mu_{22}^{neq}\nu_{12}^0 + 2\mu_{33}^{neq}\nu_{13}^0 \end{aligned} \quad (91)$$

and the initial Poisson ratios $\nu_{12}^0 := -\varepsilon_{22}^0/\varepsilon_{11}^0$ and $\nu_{13}^0 := -\varepsilon_{33}^0/\varepsilon_{11}^0$ are expressed in terms of the equilibrated and non-equilibrated reference shear moduli through —c.f.

Ref. [20]

$$\nu_{12}^0 = \frac{\mu_{33}^0}{\mu_{22}^0 + \mu_{33}^0} = \frac{\mu_{33}^{eq} + \mu_{33}^{neq}}{\mu_{22}^{eq} + \mu_{22}^{neq} + \mu_{33}^{eq} + \mu_{33}^{neq}} \quad (92)$$

$$\nu_{13}^0 = \frac{\mu_{22}^0}{\mu_{22}^0 + \mu_{33}^0} = \frac{\mu_{22}^{eq} + \mu_{22}^{neq}}{\mu_{22}^{eq} + \mu_{22}^{neq} + \mu_{33}^{eq} + \mu_{33}^{neq}} \quad (93)$$

The uniaxial stress at $t = 0^+$ is found to be

$$\sigma_{11}^0 = (2\mu_{11}^0 + \mu_{22}^0\nu_{12}^0 + \mu_{33}^0\nu_{13}^0) \varepsilon_{11}^0 =: E_{11}^0 \varepsilon_{11}^0 \quad (94)$$

where E_{11}^0 represents the instantaneous Young's modulus in direction \mathbf{e}_1 . Upon the split

$$\sigma_{11}^0 = E_{11}^{eq} \varepsilon_{11}^0 + E_{11}^{neq} \varepsilon_{\varepsilon 11}^0 \quad (95)$$

with

$$E_{11}^{eq} := 2\mu_{11}^{eq} + \mu_{22}^{eq}\nu_{12}^0 + \mu_{33}^{eq}\nu_{13}^0 \quad (96)$$

the consideration of the first component in Eq. (90) and the subsequent comparison of Eq. (94) to the expression of its time derivative $\dot{\sigma}_{11}^0$ we readily arrive to

$$\left\{ \begin{array}{l} 2 \frac{E_{11}^{neq}}{\mu_{11}^{neq}} \frac{1}{\tau_{11}} + \frac{H_{12}^{neq}}{\mu_{22}^{neq}} \frac{1}{\tau_{22}} + \frac{H_{13}^{neq}}{\mu_{33}^{neq}} \frac{1}{\tau_{33}} = \frac{9}{t_{11}^0} \left(1 + \frac{E_{11}^{eq}}{E_{11}^{neq}} \right) \\ \frac{H_{21}^{neq}}{\mu_{11}^{neq}} \frac{1}{\tau_{11}} + 2 \frac{E_{22}^{neq}}{\mu_{22}^{neq}} \frac{1}{\tau_{22}} + \frac{H_{23}^{neq}}{\mu_{33}^{neq}} \frac{1}{\tau_{33}} = \frac{9}{t_{22}^0} \left(1 + \frac{E_{22}^{eq}}{E_{22}^{neq}} \right) \\ \frac{H_{31}^{neq}}{\mu_{11}^{neq}} \frac{1}{\tau_{11}} + \frac{H_{32}^{neq}}{\mu_{22}^{neq}} \frac{1}{\tau_{22}} + 2 \frac{E_{33}^{neq}}{\mu_{33}^{neq}} \frac{1}{\tau_{33}} = \frac{9}{t_{33}^0} \left(1 + \frac{E_{33}^{eq}}{E_{33}^{neq}} \right) \end{array} \right. \quad (97)$$

where the experimental value $t_{11}^0 := -\sigma_{11}^0/\dot{\sigma}_{11}^0$ may be measured tracing the tangent to the relaxation curve $\sigma_{11}(t)$ at $t = 0^+$. In Equations (97) the values of H_{ij} and E_{ii}^{neq}

are defined as in Eq. (91) for their respective direction. Equations (97) are linear in the three independent (inverse) relaxation times $1/\tau_{11}$, $1/\tau_{22}$ and $1/\tau_{33}$. Hence, they constitute a linear system from which we can determine the relaxation times τ_{11} , τ_{22} and τ_{33} once the experimental factors t_{11}^0 , t_{22}^0 and t_{33}^0 are known (measured). The three viscosities η_{11}^d , η_{22}^d and η_{33}^d are then obtained from Eq. (62). If the three “axial” viscosities are equal, i.e. $\mu_{11}^{neq}\tau_{11} = \mu_{22}^{neq}\tau_{22} = \mu_{33}^{neq}\tau_{33} = \eta^d$, then Eq. (97)₁ is uncoupled from the other preferred directions and provides the same result obtained in Ref. [20]

$$\frac{\eta^d}{\mu_{11}^{neq}} = \tau_{11} = t_{11}^0 \frac{E_{11}^{neq}/(3\mu_{11}^{neq})}{1 + E_{11}^{eq}/E_{11}^{neq}} \quad (98)$$

For the present orthotropic case, three additional small strain shear tests are needed in order to completely characterize the present model. Since the shear components in Eq. (59) are fully uncoupled in the preferred material basis, we obtain from a simple shear relaxation test in the plane $\{\mathbf{e}_1, \mathbf{e}_2\}$ under a plane stress condition

$$\frac{\eta_{12}^d}{\mu_{12}^{neq}} = \tau_{12} = t_{12}^0 \frac{1}{1 + \mu_{12}^{eq}/\mu_{12}^{neq}} \quad (99)$$

where $t_{12}^0 := -\sigma_{12}^0/\dot{\sigma}_{12}^0$ is determined from the experimental shear stress relaxation curve $\sigma_{12}(t)$. Two homologous expressions for τ_{23} and τ_{31} are derived from the respective simple shear tests performed in the other preferred planes $\{\mathbf{e}_2, \mathbf{e}_3\}$ and $\{\mathbf{e}_3, \mathbf{e}_1\}$.

8. Examples

The following examples are designed to compare the obtained behavior against models based on the Sidoroff decomposition [13, 20] and to highlight the enhanced capabilities of the present anisotropic visco-hyperelasticity formulation based on the reverse multiplicative decomposition.

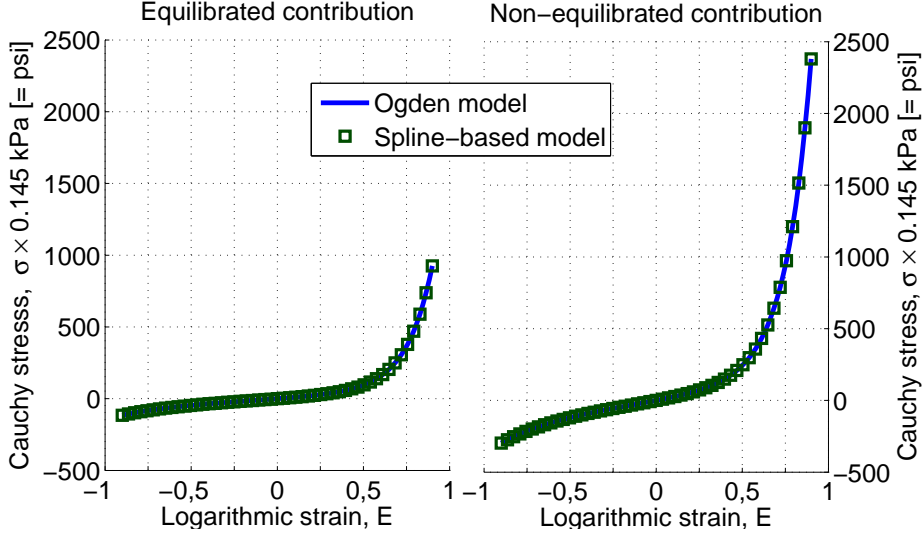


Figure 4: Uniaxial stresses derived from the equilibrated and non-equilibrated Ogden-type strain energy functions [13] and predictions using the spline-based isotropic model [27].

8.1. Isotropic material

In Ref. [20] we showed that the anisotropic model derived therein in full material description gives exactly the same results than the isotropic model of Reese and Govindjee [13] formulated in spatial principal directions when an isotropic (spline-based, Ogden-type or whatever) strain energy function is considered. Both models are based on the Sidoroff’s multiplicative decomposition. The same simple shear cyclic test simulation of the first example in Ref. [20] is performed herein, the only difference between them being the multiplicative decomposition employed in the formulation. That is, the same equilibrated and non-equilibrated deviatoric strain energy functions \mathcal{W}_{eq} and \mathcal{W}_{neq} (using the spline-based model, see Figure 4), volumetric penalty function \mathcal{U}_{eq} , relaxation time $\tau = \eta^d / \mu^{neq} = 17.5$ s and (mixed) finite element formulation are employed. We only compare the results obtained with the respective Finite (Non-Linear) Viscoelasticity formulations.

In Figure 5, the obtained Cauchy shear stresses $\sigma_{12}(t)$ are plotted against the engineering shear strains $\gamma_{12}(t)$ for three different amplitudes in the simple shear test.

Both models predict the same behavior within the context of small strains. However, the predictions given by the models separate when large shear strains are considered (note that for purely axial loadings, both models would exactly predict the same viscoelastic behavior).

Representative convergence rates for the unbalanced force and energy using a symmetric solver and an unsymmetric solver are shown in Table 1 for the case labeled (*c'*) in Figure 5. The symmetrization of the third addend in Eq. (75) and the subsequent use of a symmetric solver in the global finite element iterations are clearly justified in this case.

Step 465 Iteration	Load norm (Symmetric)	Load norm (Unsymmetric)	Energy norm (Symmetric)	Energy norm (Unsymmetric)
1	1.412E+05	1.412E+05	1.771E+04	1.771E+04
2	7.923E+00	5.307E+00	5.455E-05	1.862E-06
3	3.334E-03	1.692E-04	6.050E-11	9.427E-12

Table 1: Comparison of convergence rates using the reverse decomposition and either a symmetric solver or an unsymmetric solver. Case labeled (*c'*) in Figure 5

8.2. Orthotropic material with linear logarithmic stress-strain relations

In this example from Reference [20] uniaxial in-axis orthotropic relaxation testing is performed along different material directions. Consider the following strain energy functions

$$\mathcal{W}_{eq}(\mathbf{E}^d) = \mu_{11}^{eq}(E_{11}^d)^2 + \mu_{22}^{eq}(E_{22}^d)^2 + \mu_{33}^{eq}(E_{33}^d)^2 \quad (100)$$

$$\mathcal{W}_{neq}(\mathbf{E}_e^d) = \mu_{11}^{neq}(E_{e11}^d)^2 + \mu_{22}^{neq}(E_{e22}^d)^2 + \mu_{33}^{neq}(E_{e33}^d)^2 \quad (101)$$

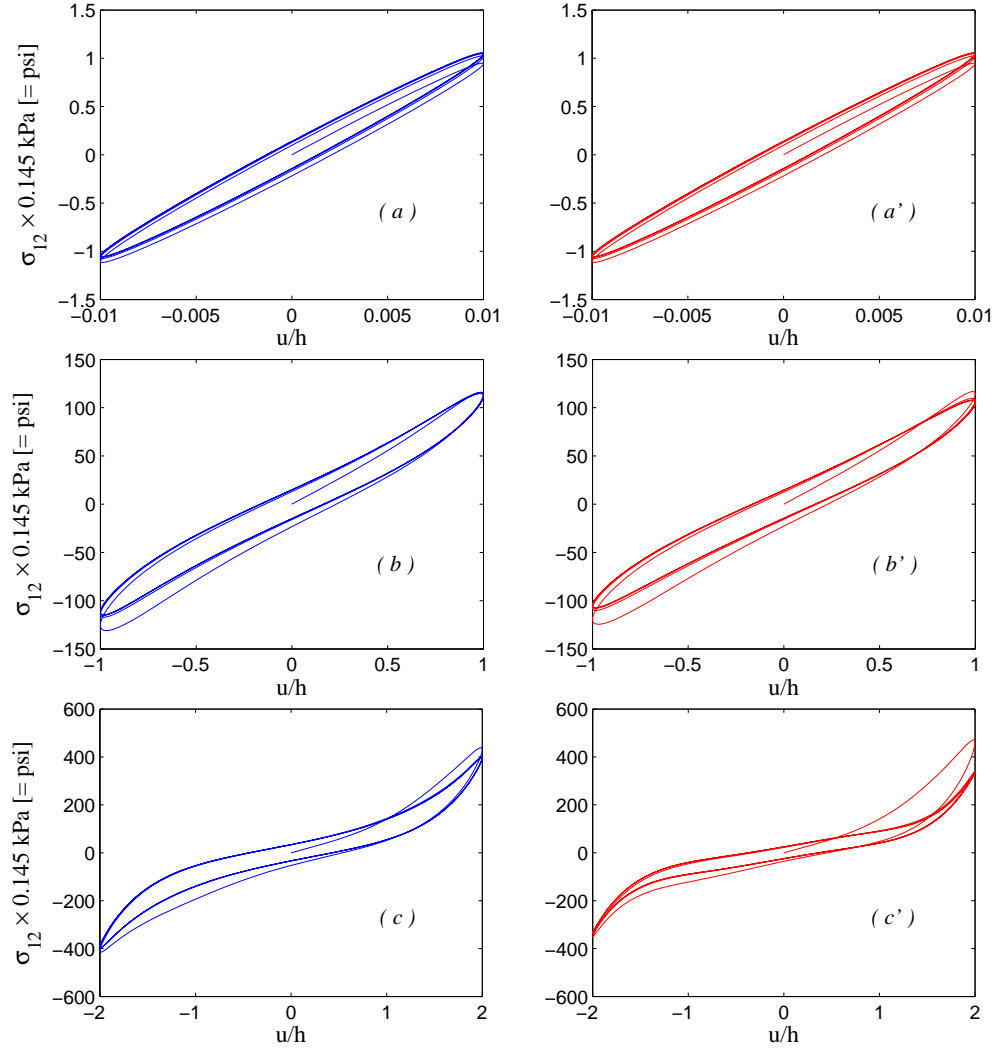


Figure 5: Cauchy shear stresses $\sigma_{12}(t)$ versus engineering shear strains $\gamma_{12}(t) = u(t)/h = u_0/h \times \sin(0.3t)$ for the amplitudes: a) a') $u_0/h = 0.01$, b) b') $u_0/h = 1$, c) c') $u_0/h = 2$. Curves a , b and c obtained using the model based on the Sidoroff decomposition as given in Ref. [20] (see also [13]). Curves a' , b' and c' are obtained using the present formulation based on the reversed decomposition. All the simulations are performed using the respective finite fully non-linear formulations (FV) (100 time steps per cycle).

where only the axial components in principal material directions are needed in order to simulate the different uniaxial relaxation tests about the preferred material axes. We take the same values for the shear moduli in Eqs. (100) and (101) used in the second example in Ref. [20]

$$\mu_{11}^{eq} = 4 \text{ MPa}, \mu_{22}^{eq} = 2 \text{ MPa}, \mu_{33}^{eq} = 1 \text{ MPa} \quad (102)$$

$$\mu_{11}^{neq} = 5 \text{ MPa}, \mu_{22}^{neq} = 3 \text{ MPa}, \mu_{33}^{neq} = 2 \text{ MPa} \quad (103)$$

In the example of Ref. [20], a single relaxation time $\tau_{11} = 20 \text{ s}$ was needed in order to complete the definition of the model. The (non-independent) relaxation times $\tau_{22} = \tau_{11} \times \mu_{11}^{neq} / \mu_{22}^{neq} = 33.3 \text{ s}$ and $\tau_{33} = \tau_{11} \times \mu_{11}^{neq} / \mu_{33}^{neq} = 50 \text{ s}$ were then obtained by the model because of the isotropy assumption in the viscous component. In the present anisotropic case we need to prescribe three independent relaxation times (the three other relaxation times for shear behavior are not needed in this example). The initially undeformed block of $100 \times 100 \times 100$ is deformed (quasi) instantaneously along material direction 1 up to a dimension of 300, whereas the other directions, due to material behavior, result in 66.2 for material direction 2 and 50.4 for material direction 3; see Ref. [20].

In the first simulation within this example we prescribe the relaxation times that give as a result the same isotropic viscosity tensor used in Ref. [20] —see Eq. (62)

$$\tau_{11} = 20 \text{ s}, \quad \tau_{22} = 33.3 \text{ s}, \quad \tau_{33} = 50 \text{ s} \quad \Rightarrow \quad \eta_{11}^d = \eta_{22}^d = \eta_{33}^d \quad (104)$$

in order to show that the same results are obtained using the model based on the Sidoroff multiplicative decomposition and the present model based on the reversed

one, both with the same isotropic viscous behavior. The same results are expected to be obtained because the loads are applied over the preferred directions of the material and no rotations are present. Hence both decompositions are indistinguishable from a numerical standpoint, i.e. $\mathbf{U} = \mathbf{U}_e \mathbf{U}_v = \mathbf{U}_v \mathbf{U}_e$. Furthermore, in this case the condition for the co-rotational rate $\dot{\mathbf{X}}_v = \mathbf{0}$ is coincident to the condition $\dot{\mathbf{X}}_v = \mathbf{0}$, whereupon the non-equilibrated tangent moduli \mathbb{C}_{neq} given in Eq. (75) preserves all the symmetries and no distinction between using a symmetric or a unsymmetric solver is needed in this example. In Figure 6 we can verify that identical stress relaxation curves (dashed lines) to those shown in Ref. [20] are obtained for the three (separate) uniaxial tests performed over the three preferred directions using the present model.

As a second case within this example we prescribe independent relaxation times in order to show the enhanced capabilities of the present model when it is used with an orthotropic viscosity tensor. The following independently user-prescribed values for the *axial* relaxation times have been chosen

$$\tau_{11} = 80 \text{ s} , \quad \tau_{22} = 100 \text{ s} , \quad \tau_{33} = 25 \text{ s} \quad \Rightarrow \quad \eta_{11}^d \neq \eta_{22}^d \neq \eta_{33}^d \neq \eta_{11}^d \quad (105)$$

In Eq. (104) the relations $\tau_{11} < \tau_{22} < \tau_{33}$ hold because $\mu_{11}^{neq} > \mu_{22}^{neq} > \mu_{33}^{neq}$, i.e. the stiffer non-equilibrated behavior in a given direction, the faster relaxation process associated to that direction. However, these restrictions do not necessarily hold in the present model, see Eq. (105). Indeed, we can observe in Figure 6 (solid lines) that in this case the material relaxes faster in direction 3 than in the other two directions. Since the same strain energy functions are used in all the simulations, the same instantaneous and relaxed states are obtained for each test, independently of the relaxation times being prescribed.

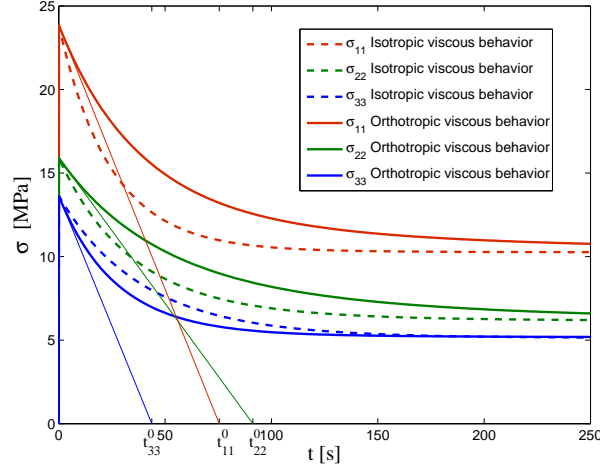


Figure 6: Dashed curves: Stress relaxation curves $\sigma_{11}(t)$, $\sigma_{22}(t)$ and $\sigma_{33}(t)$ obtained from three uniaxial relaxation tests performed about the preferred material directions 1, 2 and 3, respectively, using the model based on the reverse multiplicative decomposition and the same isotropic viscosity tensor used in the second example of Ref. [20]. Solid curves: idem using an orthotropic viscosity tensor.

Finally, introducing the material parameters given in Eqs. (102), (103) and (105) into Eqs. (97) we obtain the following values for the experimental parameters

$$t_{11}^0 = 75.5 \text{ s}, \quad t_{22}^0 = 91.3 \text{ s} \quad \text{and} \quad t_{33}^0 = 43.8 \text{ s} \quad (106)$$

We can see in Figure 6 that the values t_{11}^0 , t_{22}^0 and t_{33}^0 obtained from the computational relaxation curves are in very good agreement with the preceding values. This fact proves the applicability of the material characterization procedure explained in Section 7 to the present computational model.

8.3. Orthotropic material

In this example we perform the analysis of an orthotropic visco-hyperelastic plate with a hole, see Figure 7. The plate is loaded about the x -axis, i.e. 30 away the

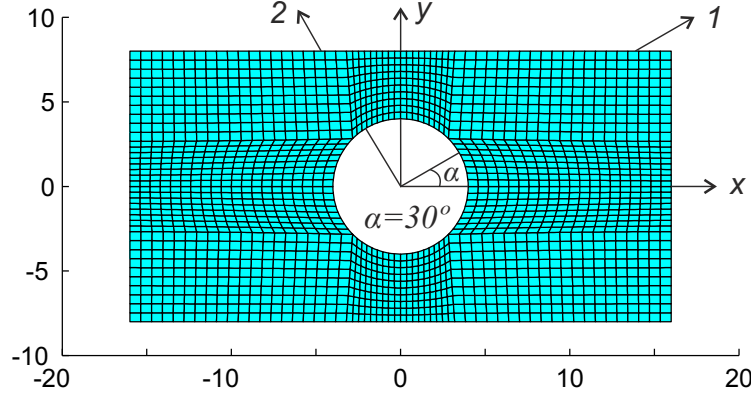


Figure 7: Rectangular plate with a concentric hole: reference configuration, initial orientation ($\alpha = 30^\circ$) of the preferred material directions and finite element mesh. Dimensions of the plate: $l_0 \times h_0 = 32 \times 16 \text{ mm}^2$. Radius of the hole: $r_0 = 4 \text{ mm}$.

principal material 1-axis. This example is the same as that given in Ref. [20]. In this case we used (bidimensional) 9/3, u/p mixed finite elements, see [1]. We have employed in the simulations the same time increments and time sequences as in Ref. [20].

The deviatoric responses of the equilibrated and non-equilibrated parts of our model are described by orthotropic spline-based strain energy functions of the type —c.f. Ref. [29]

$$\mathcal{W}_{eq}(\mathbf{E}^d) = \sum_{i=1}^3 \sum_{j=1}^3 \omega_{ij}^{eq}(E_{ij}^d) \quad (107)$$

$$\mathcal{W}_{neq}(\mathbf{E}_e^d) = \sum_{i=1}^3 \sum_{j=1}^3 \omega_{ij}^{neq}(E_{eij}^d) \quad (108)$$

whose first derivative functions are shown in Figure 8.

The preceding equilibrated and non-equilibrated stored energy functions were used in the second simulation addressed within Example 3 in Ref. [20]. Therein, the prescribed value $\tau_{11} = 10 \text{ s}$ implied $\tau_{22} = 10.23 \text{ s}$, $\tau_{33} = 23.86 \text{ s}$, $\tau_{12} = 3.78 \text{ s}$,

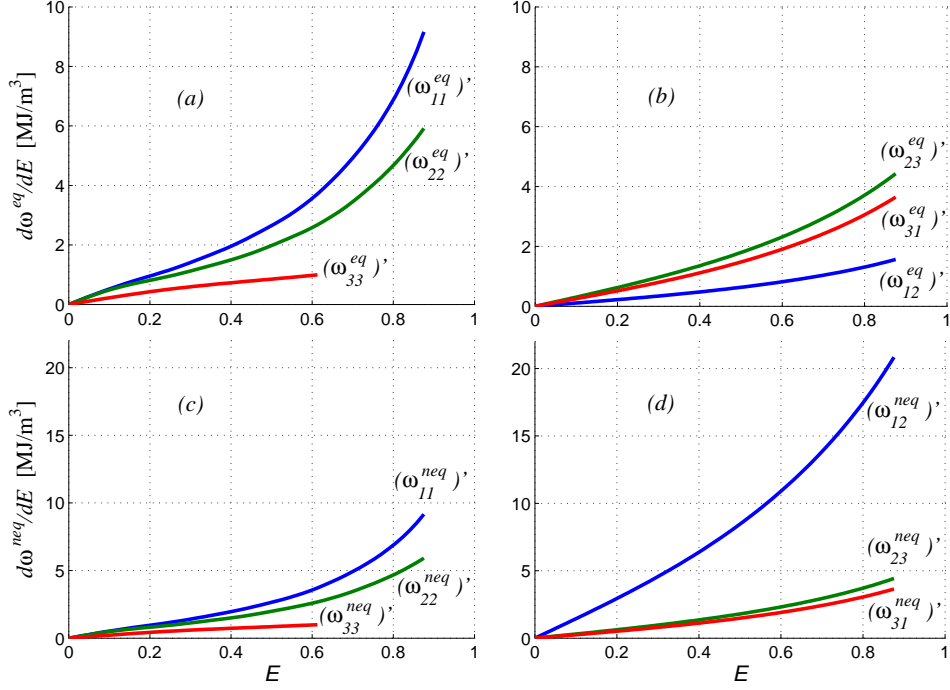


Figure 8: (a) and (b): First derivative functions of the components of the strain energy function \mathcal{W}_{eq} . (c) and (d): First derivative functions of the components of the strain energy function \mathcal{W}_{neq} . Note that the only difference between \mathcal{W}_{eq} and \mathcal{W}_{neq} is the component ω_{12} . The symmetries $\omega'_{ij}(-E_{ij}) = -\omega'_{ij}(E_{ij})$ are considered for all the functions shown in this figure.

$\tau_{23} = 17.82\text{ s}$ and $\tau_{31} = 21.63\text{ s}$, thereby $\eta_{ij}^d = \eta^d$. Even though the formulation employed in this case (based on the reversed decomposition) is different from the formulation used in Ref. [20] (based on the Sidoroff decomposition) we can see that very similar results are obtained in both cases; compare Figure 9 with Figure 13 of [20].

In the second simulation addressed in the present example we modify the relaxation time τ_{12} in order to show that with the present model we have control over the relaxation process associated to the change of the overall angular distortion from $\gamma_{xy}^0 > 0$ to $\gamma_{xy}^\infty < 0$. The values of the remaining relaxation times are preserved. The relaxation time τ_{12} is increased up to $\tau_{12} = 10\text{ s}$. As a result, note that the numerical calculations show a shear relaxation process that is slower in Figure 10 than in Figure 9. Furthermore, we observe that a complete relaxation has almost been achieved in Figure 9 at $t = 155\text{ s}$, while the plate in Figure 10 is still relaxing at that instant. Obviously, the other relaxation times could have been modified to give other very different relaxation processes, always preserving the same instantaneous and relaxed states. As a main consequence even though the present formulation is more complex, it is apparent that a wider spectrum of material behaviors may be captured with the present model than with that of Ref. [20].

Convergence rates at representative steps using a symmetric and an unsymmetric solver are shown in Table 2. It can be seen that the use of a symmetric solver results in only about one additional iteration per step.

9. Conclusions

In this paper we present a phenomenological formulation and numerical algorithm for anisotropic visco-hyperelasticity. The formulation is based on a reverse

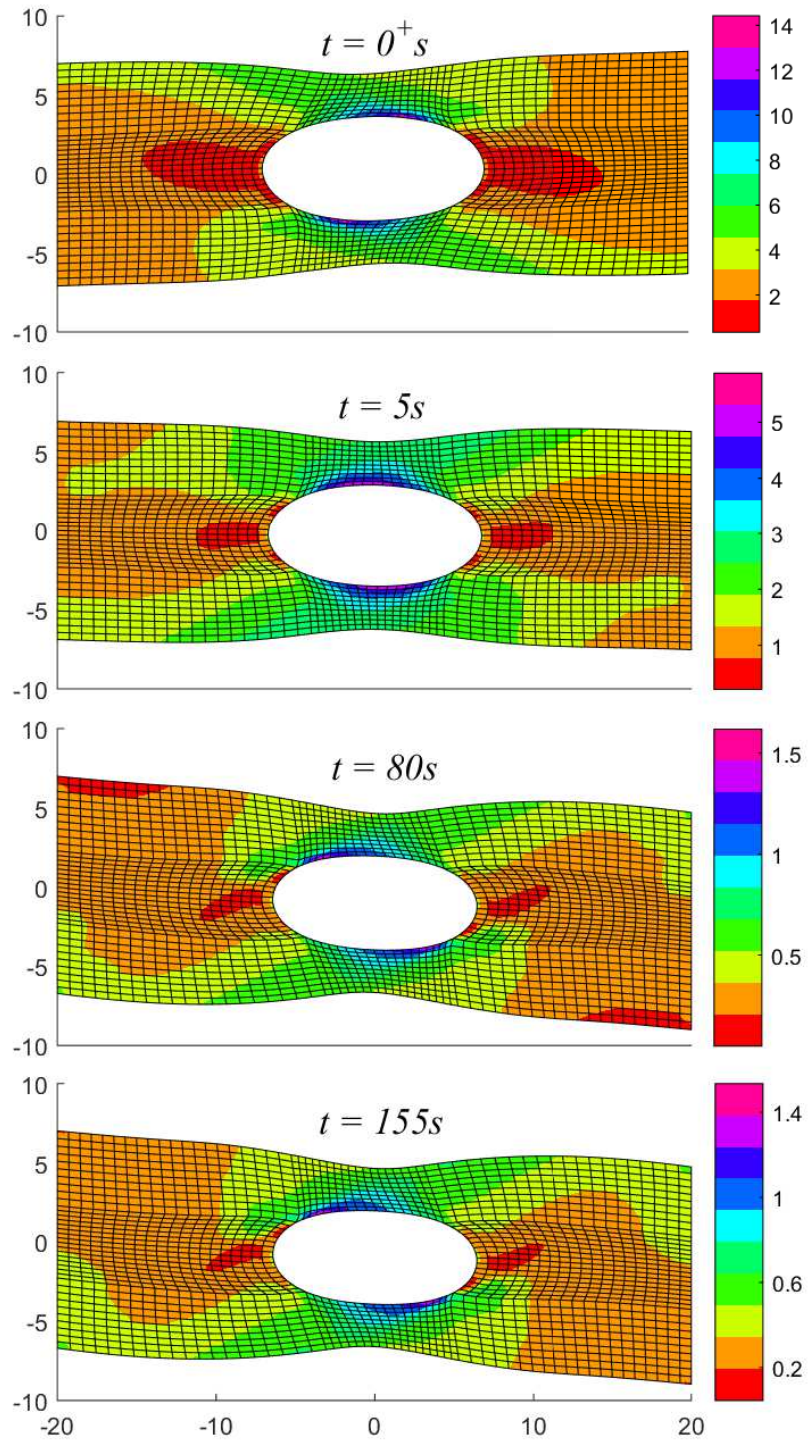


Figure 9: Relaxation process of the plate using the model based on the reverse decomposition with an isotropic viscosity tensor. Specifically, $\tau_{12} = 3.78$ s. Deformed configurations and distributions of $\|\sigma^d\|$ (MPa) at instants $t = 0^+ s$, $t = 5 s$, $t = 80 s$ and $t = 155 s$. Unaveraged results at nodes.

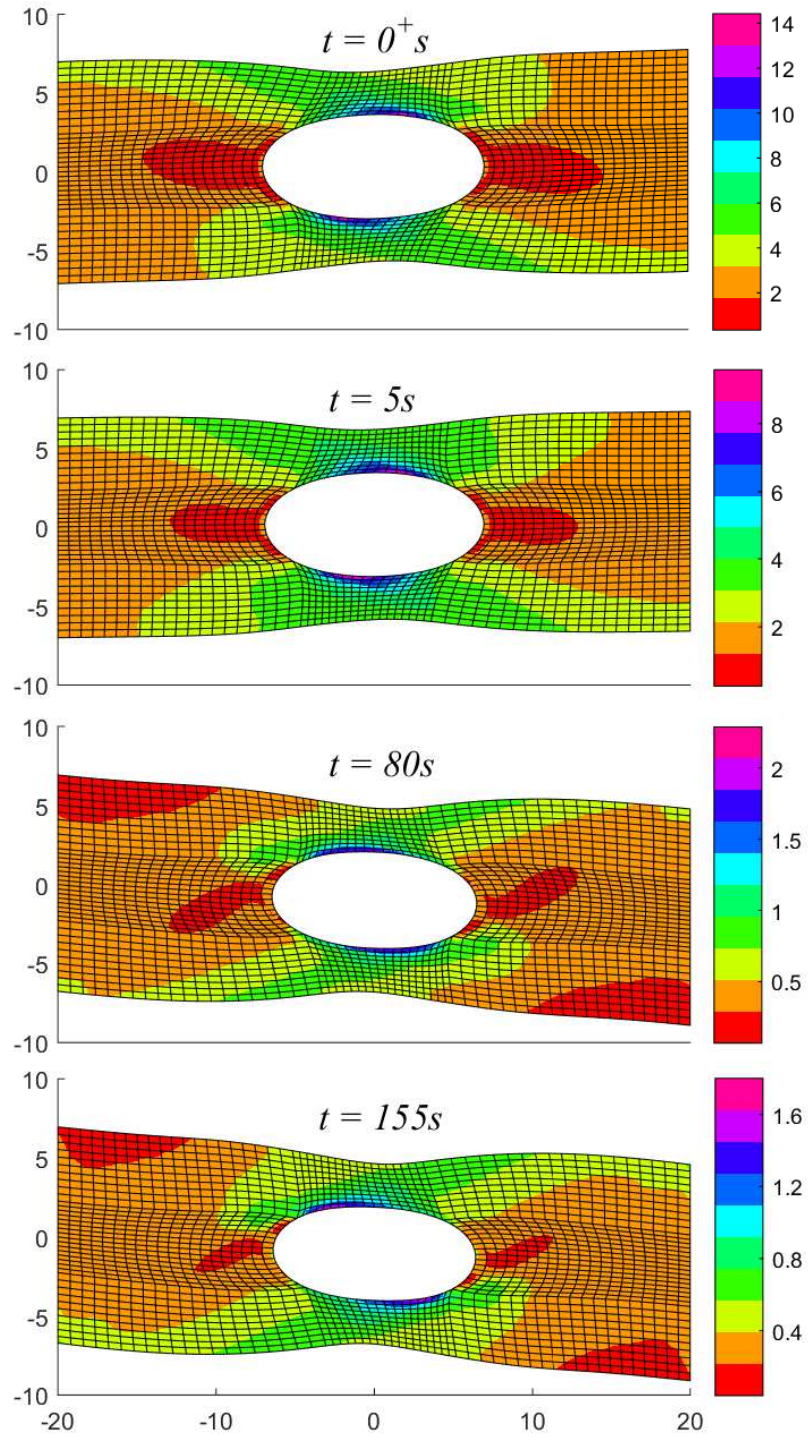


Figure 10: Relaxation process of the plate using the model based on the reversed decomposition with an anisotropic viscosity tensor. Specifically, $\tau_{12} = 10$ s. Deformed configurations and distributions of $\|\sigma^d\|$ (MPa) at instants $t = 0^+ s$, $t = 5 s$, $t = 80 s$ and $t = 155 s$. Unaveraged results at nodes.

Time (Δt)	Step (Iteration)	Load norm (Symmetric)	Load norm (Unsymmetric)	Energy norm (Symmetric)	Energy norm (Unsymmetric)
2.5 s (0.125 s)	20(1)	1.974E-01	1.974E-01	5.467E-03	5.466E-03
	20(2)	1.261E-02	1.281E-02	5.877E-07	2.872E-07
	20(3)	2.689E-05	8.682E-07	8.239E-11	1.975E-15
	20(4)	5.823E-07		3.830E-14	
20 s (1.5 s)	50(1)	7.004E-01	7.004E-01	1.339E-01	1.339E-01
	50(2)	2.286E-01	2.331E-01	1.535E-04	1.460E-04
	50(3)	3.587E-04	2.225E-04	8.429E-09	1.223E-10
	50(4)	1.054E-05	4.378E-08	7.515E-12	3.893E-17
	50(5)	4.420E-07		1.249E-14	

Table 2: Comparison of convergence rates using the reverse decomposition and either a symmetric solver or an unsymmetric solver. Example of Figure 10.

multiplicative decomposition and on a split of the stored energy into distinct anisotropic equilibrated and nonequilibrated addends. The formulation is valid for large deviations from thermodynamic equilibrium. The procedure may employ anisotropic stored energies and anisotropic viscosities. For the orthotropic case, six relaxation experiments completely define the viscosities. The procedure to obtain material parameters from experiments is also detailed. The algorithm is formulated using logarithmic stress and strain measures in order to facilitate the use of spline-based stored energies. The resulting algorithmic tangent may be slightly nonsymmetric. However, in the analyzed examples, the computational cost of using a symmetric tangent in terms of iterations is small.

Acknowledgements

Partial financial support for this work has been given by grant DPI2011-26635 from the Dirección General de Proyectos de Investigación of the Ministerio de Economía y Competitividad of Spain.

References

References

- [1] Bathe KJ (2014) Finite Element Procedures, 2nd Ed. KJ Bathe, Watertown.
- [2] Ogden RW (1997) Nonlinear Elastic Deformations. Dover, New York.
- [3] Holzapfel GA (2000) Nonlinear Solid Mechanics. A Continuum Approach For Engineering. Wiley, Chichester.
- [4] Fung YC (1993) A First Course in Continuum Mechanics. Prentice-Hall.
- [5] Kojić M, Bathe KJ (2005). Inelastic Analysis of Solids and Structures. Springer.
- [6] Simo JC, Hughes TJR (1998) Computational Inelasticity. New York, Springer.
- [7] Bonet J, Wood RD (2008). Nonlinear Continuum Mechanics for Finite Element Analysis. Cambridge.
- [8] Simo JC (1987) On a fully three-dimensional finite-strain viscoelastic damage model: formulation and computational aspects. *Comput Methods Appl Mech Eng* 60(2):153–173.
- [9] Holzapfel GA, Gasser TC, Stadler M (2002) A structural model for the viscoelastic behavior of arterial walls: continuum formulation and finite element analysis. *Eur J Mech-A/Sol* 21(3):441–463.
- [10] Holzapfel GA (1996) On large strain viscoelasticity: continuum formulation and finite element applications to elastomeric structures. *Int J Numer Methods Eng* 39(22):3903–3926.

- [11] Peña JA, Martínez MA, Peña E (2011) A formulation to model the nonlinear viscoelastic properties of the vascular tissue. *Acta Mech* 217(1-2):63–74.
- [12] Peña E, Peña JA, Doblaré M (2008) On modelling nonlinear viscoelastic effects in ligaments. *J Biomech* 41(12):2659–2666.
- [13] Reese S, Govindjee S (1998) A theory of finite viscoelasticity and numerical aspects. *Int J Sol Struct* 35(26):3455–3482.
- [14] Haslach Jr HW (2005) Nonlinear viscoelastic, thermodynamically consistent, models for biological soft tissue. *Biomech Model Mechanobiol* 3(3):172–189.
- [15] Holmes DW, Loughran JG (2010) Numerical aspects associated with the implementation of a finite strain, elasto-viscoelastic-viscoplastic constitutive theory in principal stretches. *Int J Numer Methods Eng* 83(3):366–402.
- [16] Peric D, Dettmer W (2003) A computational model for generalized inelastic materials at finite strains combining elastic, viscoelastic and plastic material behaviour. *Eng Comput* 20(5/6):768–787.
- [17] Sidoroff F (1974) Un modèle viscoélastique non linéaire avec configuration intermédiaire. *J Mécanique* 13(4):679–713.
- [18] Lubliner J (1985) A model of rubber viscoelasticity. *Mech Res Commun* 12(2):93–99.
- [19] Nguyen TD, Jones RE, Boyce BL (2007) Modeling the anisotropic finite-deformation viscoelastic behavior of soft fiber-reinforced composites. *Int J Sol Struct* 44(25):8366–8389.

- [20] Latorre M, Montáns FJ (2015) Anisotropic finite strain viscoelasticity based on the Sidoroff multiplicative decomposition and logarithmic strains. *Comput Mech* (In Press) DOI 10.1007/s00466-015-1184-8.
- [21] Latorre M, Montáns FJ (2014) On the interpretation of the logarithmic strain tensor in an arbitrary system of representation. *Int J Sol Struct* 51(7):1507–1515.
- [22] Fiala Z (2015). Discussion of “On the interpretation of the logarithmic strain tensor in an arbitrary system of representation” by M. Latorre and F.J. Montáns. *Int J Sol Struct* 56–57:290–291.
- [23] Latorre M, Montáns FJ (2015). Response to Fiala’s comments on “On the interpretation of the logarithmic strain tensor in an arbitrary system of representation”. *Int J Sol Struct* 56–57:292.
- [24] Caminero MA, Montáns FJ, Bathe KJ (2011) Modeling large strain anisotropic elasto-plasticity with logarithmic strain and stress measures. *Comput Struct* 89(11):826–843.
- [25] Montáns FJ, Benítez JM, Caminero MA (2012) A large strain anisotropic elasto-plastic continuum theory for nonlinear kinematic hardening and texture evolution. *Mech Res Commun* 43:50–56.
- [26] Eterovic AL, Bathe KJ (1990) A hyperelastic-based large strain elasto-plastic constitutive formulation with combined isotropic-kinematic hardening using the logarithmic stress and strain measures. *Int J Numer Methods Eng* 30(6):1099–1114.
- [27] Sussman T, Bathe KJ (2009) A Model of Incompressible Isotropic Hyperelas-

- tic Material Behavior using Spline Interpolations of Tension-Compression Test Data. *Commun Num Meth Eng* 25:53–63.
- [28] Latorre M, Montáns FJ (2013) Extension of the Sussman–Bathe spline-based hyperelastic model to incompressible transversely isotropic materials. *Comput Struct* 122:13–26.
- [29] Latorre M, Montáns FJ (2014) What-You-Prescribe-Is-What-You-Get orthotropic hyperelasticity. *Comput Mech* 53(6):1279–1298.
- [30] Latorre M, Montáns FJ (2015) Material-symmetries congruency in transversely isotropic and orthotropic hyperelastic materials. *Eur J Mech-A/Sol* 53:99-106.
- [31] Lee EH (1969) Elastic-plastic deformation at finite strains. *J Appl Mech* 36(1):1–6.
- [32] Bilby BA, Bullough R, Smith E (1955) Continuous distributions of dislocations: a new application of the methods of non-Riemannian geometry. *Proc R Soc Lond, Ser A, Math Phys Sci* 231(1185):263–273.
- [33] Bergström JS, Boyce MC (1998) Constitutive modeling of the large strain time-dependent behavior of elastomers. *J Mech Phys Sol* 46(5):931–954.